

# Binary Spatial Random Field Reconstruction from Non-Gaussian Inhomogeneous Time-series Observations

Shunan Sheng<sup>1</sup>, Qikun Xiang<sup>1</sup>, Ido Nevat<sup>2</sup>, and Ariel Neufeld<sup>1</sup>

<sup>1</sup>School of Physical and Mathematical Sciences, Nanyang Technological  
University, Singapore

<sup>2</sup>TUMCREATE, Singapore

## Abstract

We develop a new model for *binary spatial random field reconstruction* of a physical phenomenon which is partially observed via inhomogeneous time-series data. We consider a sensor network deployed over a vast geographical region where sensors observe temporal processes and transmit compressed observations to the Fusion Center (FC). Two types of sensors are considered; one collects *point observations* at specific time points while the other collects *integral observations* over time intervals. Subsequently, the FC uses the compressed observations to infer the spatial phenomenon modeled as a binary spatial random field. We show that the resulting posterior predictive distribution is intractable and develop a tractable two-step procedure to perform inference. First, we develop procedures to approximately perform Likelihood Ratio Tests on the time-series data, for both *point sensors* and *integral sensors*, in order to compress the temporal observations to a single bit. Second, after the compressed observations are transmitted to the FC, we develop a Spatial Best Linear Unbiased Estimator (S-BLUE) in order for the FC to reconstruct the binary spatial random field at an arbitrary spatial location. Finally, we present a comprehensive study of the performance of the proposed approaches using both synthetic and real-world experiments. A weather dataset from the National Environment Agency (NEA) of Singapore with fields including temperature and relative humidity is used in the real-world experiments to validate the proposed approaches.

## Index Terms

Binary spatial random field reconstruction, Sensor Networks, Warped Gaussian Process, Likelihood Ratio Test (LRT), Spatial Best Linear Unbiased Estimator (S-BLUE).

## I. INTRODUCTION

Wireless sensor networks (WSNs) have captivated substantial attention due to its wide applications in environmental monitoring [12], weather forecasts [10, 14, 25], surveillance [30], building monitoring [4], and automation [1]. Recent studies focus on the estimation of a single point source, like source localization [5, 18, 19, 33] and source detection [6, 17, 20, 21, 38], which generally assume independence of the observations. In this paper, we consider a WSN consisting of spatially distributed sensors with limited energy and communication bandwidth. The sensors monitor temporal processes with desired features such as precipitation, humidity, temperature, concentration of substance, etc., that are dependent on a binary spatial random field [11]. These sensors transmit compressed observations to the Fusion Center (FC) [9]. The FC then reconstructs the binary spatial random field from the transmitted data at spatial locations where no sensor is placed, based on which further decisions can be made.

Binary spatial random fields are commonly used to model ecological phenomena that take binary values, such as defoliation [13] and pest outbreak [39]. Some spatial phenomena such as volcanic activity [8] and vision perception [16] may be hard to observe directly. Therefore, in our model, we analyze temporal data generated based on the values of the binary spatial random field and seek to reconstruct the field using the temporal data as proxy. The proposed dependence structure has its application in vision research [16] where two types of neuron are activated with respect to low-pass and high-pass components in graphs. It can also be adopted in environmental monitoring problems to model spatial-temporal phenomena where the spatial phenomenon is not directly observable and only the temporal processes are observed.

In many cases, these physical processes are modeled using Gaussian Processes (GPs) [22, 35, 37]. Though GPs lead to a concise and elegant probabilistic framework that allows further nonparametric regression and classification as shown in [26], their practicality is much restricted due to their normality and exponentially decaying tails, which are inappropriate to model the categorical data [11] as well as long-tailed observations [7, 34]. To ameliorate the situation, the non-linear distortion of a GP, called the Warped Gaussian Process (WGP) [15, 27, 29, 32], is often adopted as an alternative. The warping function in a WGP can take any parametric form, like the sum of tanh functions [29] or Tukey's family of transformations used in [24] for environment monitoring. Moreover, when the warping function is strictly increasing and continuous, the marginal likelihood of the WGP is analytically tractable [29, Section 3], which

makes the WGP outweigh other non-parametric models.

The main purpose of this paper is to develop a low complexity algorithm that can reconstruct a binary spatial random field given transmitted time-series data from sensors. The binary spatial random field is modeled by a WGP with the warping function being an indicator function. Conditional on the values of the binary spatial random field, the temporal processes are modeled by WGPs following specific non-Gaussian marginal distributions. Meanwhile, two types of sensors are deployed to observe either point or integral observations. The point observations are noisy realizations of the temporal processes at some specific time points while integral observations are the sums or averages of realizations of the temporal processes over time intervals with additive noise. In the real world, point observations are commonly used to measure real-time features such as daily temperature, and integral observations are used to track cumulative features such as total daily precipitation.

The contributions of this paper are four-fold:

- 1) We propose a novel model to represent the hierarchical spatial-temporal physical phenomenon using WGPs such that the temporal processes may follow arbitrary distributions appeared in real applications.
- 2) We develop the Warped Gaussian Process Likelihood Ratio Test (WGPLRT) and the Neighborhood-density-based Likelihood Ratio Test (NLRT) tailored to approximately perform Likelihood Ratio Tests on time-series data for sensors collecting point or integral observations, respectively.
- 3) We derive the Spatial Best Linear Unbiased Estimator (S-BLUE) for aggregating outputs of Likelihood Ratio Tests and reconstructing the spatial phenomenon, which is computationally efficient.
- 4) We perform both synthetic data experiments and real-world experiments to validate our model and algorithms. In the real-world experiments, we use a weather dataset from the National Environment Agency (NEA) of Singapore that includes fields such as temperature and relative humidity to support the proposed approaches.

The rest of the paper is structured as follows. We introduce the definitions of GPs and WGPs and present the system model in Section II. We show that the posterior predictive distribution in the proposed problem is analytically intractable and motivate a two-step procedure to reconstruct the binary spatial random field in Section III. In Section IV, we develop the Warped Gaussian Process Likelihood Ratio Test (WGPLRT) and the Neighborhood-density-

based Likelihood Ratio Test (NLRT) for inferring temporal processes. Section V introduces the Spatial Best Linear Unbiased Estimator (S-BLUE) and its properties. In Section VI and VII, we showcase the proposed model and algorithm by performing experiments using synthetic and real-world datasets<sup>1</sup>, respectively. Finally, we conclude the paper in Section VIII.

## II. DEFINITIONS & SYSTEM MODEL

In this section, we introduce the definitions of Gaussian Processes (GPs) and Warped Gaussian Processes (WGPs) and present the system model. Throughout this paper, all random variables are defined on a probability space  $(\Omega, \mathcal{F}, \mathbb{P})$ . Let us first state the definition of a GP<sup>2</sup>.

**Definition 1** (Gaussian Process (see, e.g., [26, Definition 2.1])).

Let  $\mathcal{X} \subseteq \mathbb{R}^d$  and let  $f : \Omega \times \mathcal{X} \rightarrow \mathbb{R}$  denote a stochastic process parametrized by  $\mathbf{x} \in \mathcal{X}$ . Then,  $f$  is a Gaussian Process (GP) with the mean function  $\mu : \mathcal{X} \rightarrow \mathbb{R}$  and the covariance function  $\mathcal{C} : \mathcal{X} \times \mathcal{X} \rightarrow \mathbb{R}$ , i.e.,  $f \sim \mathcal{GP}(\mu(\cdot), \mathcal{C}(\cdot, \cdot))$ , if all its finite dimensional distributions are Gaussian, that is, for any  $m \in \mathbb{N}$  and  $\mathbf{x}_{1:m} := (\mathbf{x}_1, \dots, \mathbf{x}_m) \in \mathcal{X}^m$ , the random variables  $(f(\mathbf{x}_1), \dots, f(\mathbf{x}_m))^T$  are jointly normally distributed with mean  $\mu(\mathbf{x}_{1:m}) := (\mu(\mathbf{x}_1), \dots, \mu(\mathbf{x}_m))^T \in \mathbb{R}^m$  and covariance matrix  $\mathcal{C}(\mathbf{x}_{1:m}, \mathbf{x}_{1:m}) \in \mathbb{R}^{m \times m}$  where  $(\mathcal{C}(\mathbf{x}_{1:m}, \mathbf{x}_{1:m}))_{i,j} := \mathcal{C}(\mathbf{x}_i, \mathbf{x}_j)$  for  $1 \leq i, j \leq m$ .

We can therefore characterize a GP by the following class of random functions:

$$\mathfrak{F} := \{f : \Omega \times \mathcal{X} \rightarrow \mathbb{R} \text{ s.t. } f \sim \mathcal{GP}(\mu(\cdot), \mathcal{C}(\cdot, \cdot)),$$

$$\text{with } \mu : \mathcal{X} \rightarrow \mathbb{R}, \mathbf{x} \mapsto \mathbb{E}[f(\mathbf{x})],$$

$$\mathcal{C} : \mathcal{X} \times \mathcal{X} \rightarrow \mathbb{R}, (\mathbf{x}, \mathbf{x}') \mapsto \mathbb{E}[(f(\mathbf{x}) - \mu(\mathbf{x}))(f(\mathbf{x}') - \mu(\mathbf{x}'))].$$

Subsequently, we define a Warped Gaussian Process (WGP) as the point-wise transformation of a GP, as detailed below.

**Definition 2** (Warped Gaussian Process).

Let  $z : \Omega \times \mathcal{X} \rightarrow \mathbb{R}$  be a stochastic process indexed by  $\mathbf{x} \in \mathcal{X} \subseteq \mathbb{R}^d$ . We call  $z$  a Warped

<sup>1</sup>Codes implemented in MATLAB can be found on GitHub: <https://github.com/ShunanSheng/WarpedGaussianProcesses>.

<sup>2</sup>We use Gaussian Process and Gaussian random field interchangeably.

*Gaussian Process (WGP) if it is the point-wise transformation of a GP  $f : \Omega \times \mathcal{X} \rightarrow \mathbb{R}$  under a Borel-measurable warping function  $W : \mathbb{R} \rightarrow \mathbb{R}$ , that is,*

$$z(\mathbf{x}) = W\left(f(\mathbf{x})\right) \quad \text{for all } \mathbf{x} \in \mathcal{X}.$$

A candidate for the warping function is  $W = F^{-1} \circ \Phi$ , where  $F$  is the cumulative distribution function (CDF) of a random variable,  $F^{-1}(u) := \inf \{x \in \mathbb{R} : F(x) \geq u\}$  for  $u \in [0, 1]$  is the Generalized Inverse of  $F$ , and  $\Phi$  is the CDF of the standard normal distribution  $\mathcal{N}(0, 1)$ . Consequently, if  $f \sim \mathcal{GP}(0, \mathcal{C}(\cdot, \cdot))$  with  $\mathcal{C}(\mathbf{x}, \mathbf{x}) = 1$  for all  $\mathbf{x} \in \mathcal{X}$ , then the CDF of  $z(\mathbf{x})$  is  $F$  for all  $\mathbf{x} \in \mathcal{X}$ .

Having formally defined the semi-parametric class of WGP models, we proceed with presenting our system model. The system model consists of the two following parts:

- 1) The physical phenomenon: a collection of spatial-temporal random processes including a binary spatial random field and a collection of temporal processes whose characteristics are based on the local values of the binary spatial field<sup>3</sup> (see (TP1) and (TP2) below).
- 2) The sensor network: a wireless sensor network is deployed to observe the local temporal processes at specific spatial locations. The wireless sensor network consists of two types of sensors: the first collects point observations of the temporal process at specific time points (see (SN2) below); the second collects integral observations of the temporal process over time intervals (see (SN3) below).

We now present the system model:

\_\_\_\_\_ Binary spatial random field \_\_\_\_\_

(BSF1) Consider a latent spatial random field  $g : \Omega \times \mathcal{X} \rightarrow \mathbb{R}$  defined over  $\mathcal{X} \subset \mathbb{R}^2$ , which is modeled as a GP with mean function  $\mu(\cdot)$  and covariance function  $\mathcal{C}(\cdot, \cdot)$ , that is

$$g \sim \mathcal{GP}\left(\mu(\cdot), \mathcal{C}(\cdot, \cdot)\right). \quad (1)$$

(BSF2) The binary spatial random field  $y : \Omega \times \mathcal{X} \rightarrow \{0, 1\}$  is defined to be the point-wise transformation of the latent spatial random field  $g$  such that

$$y(\mathbf{x}) := \mathbb{1}_{\{g(\mathbf{x}) \geq c\}}, \quad (2)$$

where  $c \in \mathbb{R}$  is a constant threshold.

<sup>3</sup>We use binary spatial random field and binary spatial field interchangeably.

---

Temporal processes

---

(TP1) At each spatial location  $\mathbf{x} \in \mathcal{X}$ , let  $f(\cdot; \mathbf{x}) : \Omega \times [0, T] \rightarrow \mathbb{R}$  be a temporal latent GP for some  $T > 0$  with characteristics depending on the value of  $y(\mathbf{x})$  such that

$$f(\cdot; \mathbf{x}) \sim \begin{cases} \mathcal{GP}(0, \mathcal{C}_0(\cdot, \cdot)), & \text{if } y(\mathbf{x}) = 0, \\ \mathcal{GP}(0, \mathcal{C}_1(\cdot, \cdot)), & \text{if } y(\mathbf{x}) = 1, \end{cases} \quad (3)$$

where  $\mathcal{C}_i : [0, T] \times [0, T] \rightarrow \mathbb{R}$ , for  $i = 0, 1$ , are the covariance functions of the respective temporal processes with  $\mathcal{C}_i(t, t) = 1$  for all  $t \in [0, T]$ . Given any finite collection of spatial locations, such as  $\mathbf{x}_1, \dots, \mathbf{x}_n \in \mathcal{X}$  for  $n \in \mathbb{N}$ , the random variables  $f(\cdot; \mathbf{x}_1), \dots, f(\cdot; \mathbf{x}_n)$  are assumed to be independent conditional on  $(g(\mathbf{x}_1), \dots, g(\mathbf{x}_n))$ .

(TP2) The temporal process at  $\mathbf{x}$  is defined to be a WGP  $\tilde{z}(\cdot; \mathbf{x}) : \Omega \times [0, T] \rightarrow \mathbb{R}$  via a point-wise transformation of  $f$ , depending on the value of  $y(\mathbf{x})$  such that

$$\tilde{z}(t; \mathbf{x}) := \begin{cases} W_0(f(t; \mathbf{x})), & \text{if } y(\mathbf{x}) = 0, \\ W_1(f(t; \mathbf{x})), & \text{if } y(\mathbf{x}) = 1, \end{cases} \quad (4)$$

where  $W_i = F_i^{-1} \circ \Phi$ , for  $i = 0, 1$ . Each  $F_i$  is the cumulative distribution function (CDF) of a random variable,  $F_i^{-1}$  is the Generalized Inverse of  $F_i$ , and  $\Phi$  is the CDF of the standard normal distribution  $\mathcal{N}(0, 1)$ .

---

Sensor network

---

(SN1) Let  $N \in \mathbb{N}$  be the total number of sensors that are deployed over the 2-dimensional space  $\mathcal{X} \subseteq \mathbb{R}^2$  to make observations over the time period  $[0, T]$ . There are two types of sensors that are referred to as Point sensors (abbreviated to P-sensors) and Integral sensors (abbreviated to I-sensors). We assume that there are  $N^P$  P-sensors deployed at  $(\mathbf{x}_n^P)_{n=1:N^P}$  and  $N^I$  I-sensors deployed at  $(\mathbf{x}_n^I)_{n=1:N^I}$ , where  $N^P, N^I \in \mathbb{N}$  and  $N^P + N^I = N$ . Note that  $\{f(\cdot; \mathbf{x}_n^P)\}_{n=1:N^P}, \{f(\cdot; \mathbf{x}_n^I)\}_{n=1:N^I}$  are independent conditional on  $(g(\mathbf{x}_1^P), \dots, g(\mathbf{x}_{N^P}^P), g(\mathbf{x}_1^I), \dots, g(\mathbf{x}_{N^I}^I))$ .

(SN2) Point sensors: Point sensors collect noisy observations of the temporal process at the time instants  $(t_k)_{k=1}^M \subset [0, T]$  for some  $M \in \mathbb{N}$ . At each time instant  $t_k$ , the  $n$ -th P-sensor makes a noisy observation, which is given by

$$z_{n,k}^P := \tilde{z}(t_k; \mathbf{x}_n^P) + \epsilon_{n,k}^P, \quad (5)$$

where  $\epsilon_{n,1}^P, \dots, \epsilon_{n,M}^P \stackrel{i.i.d.}{\sim} \mathcal{N}(0, \sigma_P^2)$  for some noise variance  $\sigma_P^2 > 0$  with  $\epsilon_{n,k}^P$  and  $\tilde{z}(t_k; \mathbf{x}_n^P)$  being independent for all  $k = 1, \dots, M$ .

(SN3) Integral sensors: Integral sensors collect integral observations of the temporal process over consecutive time intervals  $[\frac{(k-1)T}{K}, \frac{kT}{K}]$  for  $k = 1, \dots, K$ , for some fixed  $K \in \mathbb{N}$ . The noisy observation at  $\mathbf{x}_n^I$  over the time interval  $[\frac{(k-1)T}{K}, \frac{kT}{K}]$  is given by

$$z_{n,k}^I := \int_{\frac{(k-1)T}{K}}^{\frac{kT}{K}} \tilde{z}(t; \mathbf{x}_n^I) dt + \epsilon_{n,k}^I, \quad (6)$$

where  $\epsilon_{n,1}^I, \dots, \epsilon_{n,K}^I \stackrel{i.i.d.}{\sim} \mathcal{N}(0, \sigma_I^2)$  for some noise variance  $\sigma_I^2 > 0$  with  $\epsilon_{n,k}^I$  and  $\tilde{z}(t; \mathbf{x}_n^I)$  being independent for all  $t \in [0, T]$ .

Symbol	Interpretation
$\mathbf{x}_n^P \in \mathcal{X}$	The spatial location of the $n$ -th P-sensor for $n = 1, \dots, N^P$
$\mathbf{x}_n^I \in \mathcal{X}$	The spatial location of the $n$ -th I-sensor for $n = 1, \dots, N^I$
$X_{1:N} := (\mathbf{x}_1^P, \dots, \mathbf{x}_{N^P}^P, \mathbf{x}_1^I, \dots, \mathbf{x}_{N^I}^I)$	The spatial locations of the $N$ sensors deployed in the field
$T_{1:M}^P := (t_1, \dots, t_M)$	The time instants at which the P-sensors collect observations
$T_{1:K}^I := \left\{ \left[ \frac{(k-1)T}{K}, \frac{kT}{K} \right] \right\}_{k=1}^K$	The time intervals during which the I-sensors collect observations
$\mathbf{g} := g(X_{1:N})$	The realizations of the latent spatial random field $g$ at $X_{1:N}$
$y_n^P := y(\mathbf{x}_n^P)$	The realization of the binary spatial random field $y$ at $\mathbf{x}_n^P$
$y_n^I := y(\mathbf{x}_n^I)$	The realization of the binary spatial random field $y$ at $\mathbf{x}_n^I$
$\mathbf{Z}_n^P := (z_{n,1}^P, \dots, z_{n,M}^P)^\top$	The collection of the point observations at $\mathbf{x}_n^P$ over $T_{1:M}^P$
$\tilde{\mathbf{Z}}_n^P := (\tilde{z}_{n,1}^P, \dots, \tilde{z}_{n,M}^P)^\top$	The ground-truth values of the point observations at $\mathbf{x}_n^P$ over $T_{1:M}^P$
$\mathbf{Z}_n^I := (z_{n,1}^I, \dots, z_{n,K}^I)^\top$	The collection of the integral observations at $\mathbf{x}_n^I$ over $T_{1:K}^I$
$\tilde{\mathbf{Z}}_n^I := (\tilde{z}_{n,1}^I, \dots, \tilde{z}_{n,K}^I)^\top$	The ground-truth values of the integral observations at $\mathbf{x}_n^I$ over $T_{1:K}^I$

Table I: Symbols used in the following sections.

A comprehensive list of symbols used in the following sections is provided in Table I and the graphical structure of the proposed model encoding conditional independence relations is presented in Figure 1 as a directed acyclic-graph (DAG) using plate notations. The main objective of this paper is **Binary spatial random field reconstruction**, abbreviated as **Spatial field reconstruction**. In other words, given an un-monitored location  $\mathbf{x}_* \in \mathcal{X}$ , we want to infer the value of the binary spatial random field  $y_* := y(\mathbf{x}_*)$  based on the data transmitted by the  $N$  sensors.

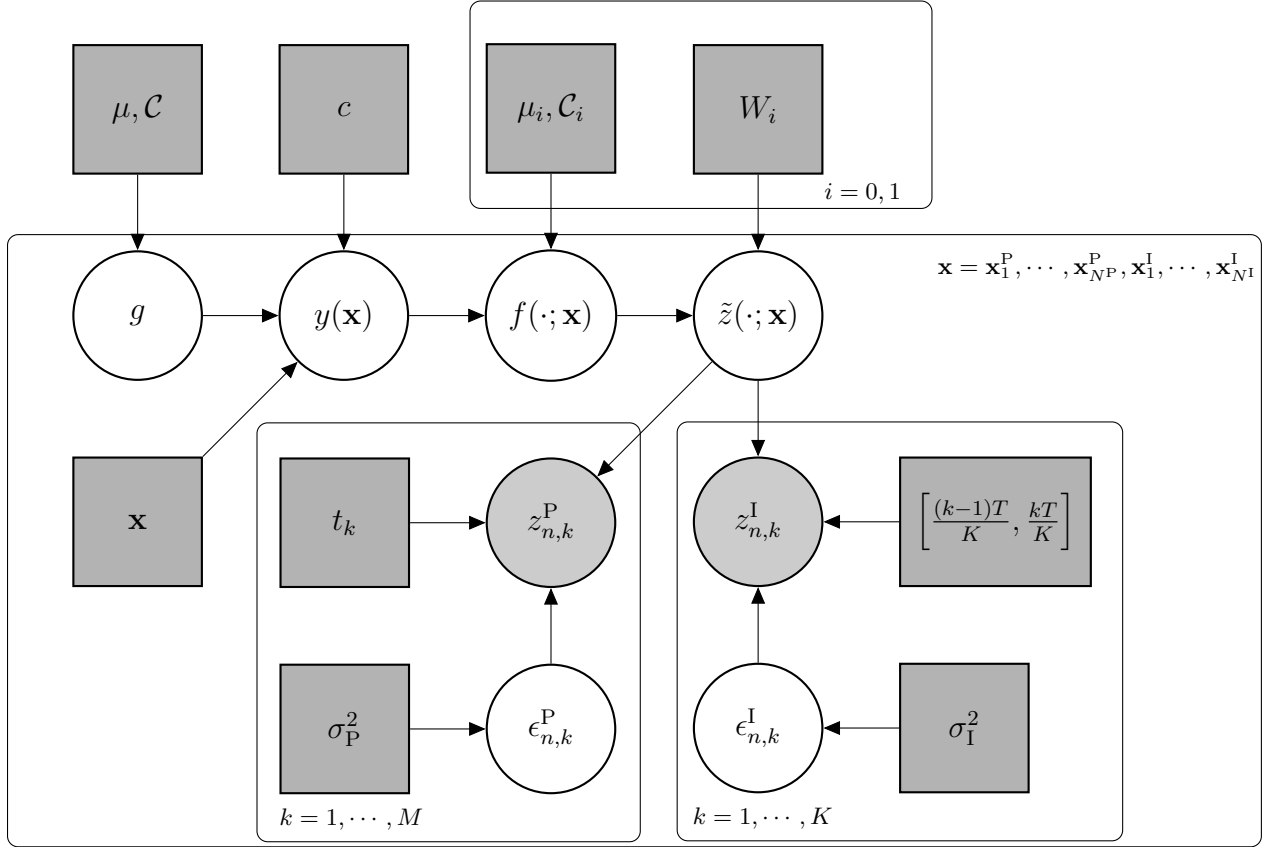


Figure 1: Directed acyclic graph (DAG) of the model encoding conditional independence relations using plate notations. The shaded rectangles represent the constants and observed covariates. The white circles indicate the latent variables. The shaded circles ensemble the observed random variables.

**Remark 3.** If  $\mu(\mathbf{x}) = 0$  and  $\mathcal{C}(\mathbf{x}, \mathbf{x}) = 1$  for all  $\mathbf{x} \in \mathcal{X}$ , then the binary spatial random field satisfies  $y(\mathbf{x}) = \mathbb{1}_{\{g(\mathbf{x}) \geq c\}} = F_B^{-1}(\Phi(g(\mathbf{x})))$ ,  $\mathbb{P}$ -a.s., where  $F_B^{-1}$  is the Generalized Inverse of Bernoulli( $\pi$ ) with  $\pi = 1 - \Phi(c)$ .

**Assumption 4.** Throughout this paper, we assume that:

1) the integral observations in (SN3) are well-defined, that is,

$$\int_{\frac{(k-1)T}{K}}^{\frac{kT}{K}} |\tilde{z}(t; \mathbf{x}_n^I)| dt < \infty \quad \text{for all } k = 1, \dots, K, n = 1, \dots, N^I.$$

2) all covariance functions are symmetric and positive definite (see details in [26, Section 2.1]).

### III. POSTERIOR PREDICTIVE DISTRIBUTION & OUR APPROACH

In this section, we introduce the posterior predictive distribution for inferring the values of the binary spatial random field and highlight its computational intractability in (7). The posterior predictive distribution of  $y_* := y(\mathbf{x}_*)$  at some un-monitored spatial location  $\mathbf{x}_*$  given the Gaussian prior on  $\mathbf{g}$ , defined by  $\mathbf{g} \sim \mathcal{N}(\mu(X_{1:N}), \mathcal{C}(X_{1:N}, X_{1:N}))$ , as well as the sensor observations  $(\mathbf{Z}_{1:N^P}^P, \mathbf{Z}_{1:N^I}^I)$  is presented in the following Proposition.

**Proposition 5** (Posterior predictive distribution).

The posterior predictive distribution of  $y_*$  given the sensor observations  $(\mathbf{Z}_{1:N^P}^P, \mathbf{Z}_{1:N^I}^I)$  is Bernoulli( $\pi_*$ ) with  $\pi_*$  given by:

$$\pi_* := \int_{\mathcal{C}} \int_{\mathbb{R}^N} p(g_* | \mathbf{g}) \frac{(\prod_{n=1}^{N^P} p(\mathbf{Z}_n^P | \mathbf{g})) (\prod_{n=1}^{N^I} p(\mathbf{Z}_n^I | \mathbf{g})) p(\mathbf{g})}{\int_{\mathbb{R}^N} (\prod_{n=1}^{N^P} p(\mathbf{Z}_n^P | \mathbf{g}')) (\prod_{n=1}^{N^I} p(\mathbf{Z}_n^I | \mathbf{g}')) p(\mathbf{g}') d\mathbf{g}'} d\mathbf{g} dg_*. \quad (7)$$

Moreover, the term

$$\int_{\mathbb{R}^N} (\prod_{n=1}^{N^P} p(\mathbf{Z}_n^P | \mathbf{g}')) (\prod_{n=1}^{N^I} p(\mathbf{Z}_n^I | \mathbf{g}')) p(\mathbf{g}') d\mathbf{g}'$$

in (7) contains a sum of  $2^{N^I+N^P}$  terms, and hence is computationally intractable.

*Proof.* See Appendix A. □

Despite the fact that the Bernoulli parameter  $\pi_*$  of the posterior predictive distribution is computationally intractable, the conditional independence of  $\mathbf{Z}_n^P, \mathbf{Z}_n^I$  given  $\mathbf{g}$  motivates us to process raw observations at each sensor and aggregate the processed data at the Fusion Center. Specifically, we adopt the following two-step approach to circumvent the difficulty of evaluating the computationally intractable posterior predictive distribution.

- Step 1: For  $n = 1, \dots, N$ , the  $n$ -th sensor performs inference based on its observations of the temporal process and transmits a binary decision  $\hat{y}_n^j$  as an estimator of  $y_n^j$ ,  $j \in \{P, I\}$ . The decision process for Point sensors is detailed in Section IV-A and Algorithm 1, and the decision process for Integral sensors is detailed in Section IV-B and Algorithm 2.
- Step 2: The fusion center collects all the binary decisions from the sensors, denoted by  $\hat{\mathbf{Y}}_{1:N} = (\hat{y}_1^P, \dots, \hat{y}_{N^P}^P, \hat{y}_1^I, \dots, \hat{y}_{N^I}^I)^\top$ , and applies the Spatial Best Linear Unbiased Estimator (S-BLUE) to aggregate the results and predict  $y_* = y(\mathbf{x}_*)$  at an un-monitored location  $\mathbf{x}_*$ . This is detailed in Section V and Algorithm 3.

#### IV. STEP 1 : LOCAL BINARY DECISIONS VIA LIKELIHOOD RATIO TESTS

To make a binary decision, it is natural to use the Likelihood Ratio Test as it is the uniformly most powerful test given a fixed significance level (see, e.g., [23, Section III (a)]). Let us first model the decision problem into a hypothesis testing problem. At the spatial location  $\mathbf{x}_n^j$  for  $j \in \{P, I\}$ , the null and alternative hypotheses are given by

$$\mathcal{H}_0 : y(\mathbf{x}_n^j) = 0 \quad \text{and} \quad \mathcal{H}_1 : y(\mathbf{x}_n^j) = 1.$$

Let  $p(\mathbf{Z}_n^j | \mathcal{H}_i)$ ,  $i = 0, 1$ , denote the marginal likelihood of  $\mathbf{Z}_n^j$  under the hypothesis  $\mathcal{H}_i$  and let  $\gamma^I, \gamma^P > 0$  be the test thresholds for the P-sensors and the I-sensors, respectively. The Likelihood Ratio Test uses the following test statistic :

$$\Lambda(\mathbf{Z}_n^j) = \frac{p(\mathbf{Z}_n^j | \mathcal{H}_0)}{p(\mathbf{Z}_n^j | \mathcal{H}_1)} \underset{\mathcal{H}_1}{\overset{\mathcal{H}_0}{\geq}} \gamma^j \quad \text{for } j \in \{P, I\}. \quad (8)$$

In the following subsections, we propose two methods for approximating the LRT. Specifically, we propose the Warped Gaussian Process Likelihood Ratio Test (WGPLRT) for point observations and we propose the Neighborhood-density-based Likelihood Ratio Test (NLRT) for integral observations.

##### A. Local binary decisions for point observations

In this subsection, we present the algorithm called **Warped Gaussian Process Likelihood Ratio Test (WGPLRT)** for performing local inferences at the Point sensors. The WGPLRT exploits the Laplace Approximation to estimate the marginal likelihood function of point observations and provides a formula to approximate the test statistic defined in (8).

To begin with, the following Proposition gives the analytic expression for the marginal likelihood of  $\mathbf{Z}_n^P$  under  $\mathcal{H}_0$  and  $\mathcal{H}_1$ .

**Proposition 6** (Marginal likelihood of  $p(\mathbf{Z}_n^P | \mathcal{H}_i)$ ).

For  $i = 0, 1$ , assume that the warping function is  $W_i = F_i^{-1} \circ \Phi$  where  $F_i$  is strictly increasing and is the CDF of a continuous random variable with continuous density. Let  $G_i := \Phi^{-1} \circ F_i$  be the inverse of  $W_i$  and let  $K_i := \mathcal{C}_i(T_{1:M}^P, T_{1:M}^P) \in \mathbb{R}^{M \times M}$  be the covariance matrix evaluated

at  $T_{1:M}^P$ . Let  $\boldsymbol{\epsilon}_n^P = (\epsilon_{n,1}^P, \dots, \epsilon_{n,M}^P)^\top$  be the additive noise at  $\mathbf{x}_n^P$ . Then, the marginal likelihood at  $n$ -th  $P$ -sensor is given by

$$p(\mathbf{Z}_n^P | \mathcal{H}_i) = \int_{\mathbb{R}^M} \exp \left( -\frac{1}{2} G_i(\mathbf{Z}_n^P - \boldsymbol{\epsilon}_n^P)^\top K_i^{-1} G_i(\mathbf{Z}_n^P - \boldsymbol{\epsilon}_n^P) - \frac{1}{2} \log \det K_i - \frac{M}{2} \log 2\pi \right. \\ \left. + \sum_{m=1}^M \log \frac{\partial G_i(z)}{\partial z} \Big|_{z_{n,m}^P - \epsilon_{n,m}^P} \right) (2\pi\sigma_P^2)^{-\frac{M}{2}} \exp \left( -\frac{1}{2} \sigma_P^{-2} (\boldsymbol{\epsilon}_n^P)^\top \boldsymbol{\epsilon}_n^P \right) d\boldsymbol{\epsilon}_n^P. \quad (9)$$

*Proof.* See Appendix B. □

When the sensor observes the ground-truth values of the temporal process without observation errors, i.e.,  $\mathbf{Z}_n^P = \tilde{\mathbf{Z}}_n^P$ , then the marginal likelihood  $p(\mathbf{Z}_n^P | \mathcal{H}_i)$  for  $i = 0, 1$  in (9) reduces to the case suggested in Section 3 in [29].

However, the marginal likelihood in (9) is computationally intractable as the integrand cannot be expressed as the probability density function of a multivariate normal distribution. Our approach is to approximate the inner term involving  $G_i(\mathbf{Z}_n^P - \boldsymbol{\epsilon}_n^P)$  using the **Laplace approximation**. The details of the Laplace approximation as well as the approximated marginal likelihood function of  $p(\mathbf{Z}_n^P | \mathcal{H}_i)$  is given by the following Proposition.

**Proposition 7** (Laplace approximation).

For  $i = 0, 1$ , let

$$(\text{range}(W_i))^M \ni (v_1, \dots, v_M)^\top = \mathbf{v} \mapsto Q_i(\mathbf{v}) := -\frac{1}{2} G_i(\mathbf{v})^\top K_i^{-1} G_i(\mathbf{v}) + \sum_{m=1}^M \log \frac{\partial G_i(v)}{\partial v} \Big|_{v_m}, \quad (10)$$

where  $K_i := \mathcal{C}_i(T_{1:M}^P, T_{1:M}^P)$  for  $i = 0, 1$  are defined as in Proposition 6. Assume that there is a  $\hat{\mathbf{v}}_i \in (\text{range}(W_i))^M$  satisfying the following conditions:

- 1)  $\hat{\mathbf{v}}_i$  maximises  $Q_i$ ;
- 2)  $\hat{\mathbf{v}}_i$  is in the interior of  $(\text{range}(W_i))^M$ ;
- 3)  $Q_i$  is twice differentiable at  $\hat{\mathbf{v}}_i$ ;
- 4)  $A_i := -\nabla^2 Q_i(\mathbf{v})|_{\mathbf{v}=\hat{\mathbf{v}}_i}$  is positive definite.

Moreover, let  $Q_i(\mathbf{v})$  be approximated by its second-order Taylor polynomial as

$$\hat{Q}_i(\mathbf{v}) := -\frac{1}{2} (\mathbf{v} - \hat{\mathbf{v}}_i)^\top A_i (\mathbf{v} - \hat{\mathbf{v}}_i) + Q_i(\hat{\mathbf{v}}_i), \quad \mathbf{v} \in (\text{range}(W_i))^M, \quad (11)$$

and the approximated marginal likelihood function be given by

$$\begin{aligned} \widehat{p}(\mathbf{Z}_n^{\text{P}}|\mathcal{H}_i) &:= \int_{\mathbb{R}^M} \exp\left(\widehat{Q}_i(\mathbf{Z}_n^{\text{P}} - \boldsymbol{\epsilon}_n^{\text{P}}) - \frac{1}{2} \log \det K_i - \frac{M}{2} \log 2\pi\right) \\ &\quad \times (2\pi\sigma_{\text{P}}^2)^{-\frac{M}{2}} \exp\left(-\frac{1}{2}\sigma_{\text{P}}^{-2}(\boldsymbol{\epsilon}_n^{\text{P}})^{\text{T}}\boldsymbol{\epsilon}_n^{\text{P}}\right) \text{d}\boldsymbol{\epsilon}_n^{\text{P}}. \end{aligned} \quad (12)$$

Then,

$$\widehat{p}(\mathbf{Z}_n^{\text{P}}|\mathcal{H}_i) = \widehat{C}_i \exp\left(-\frac{1}{2}(\mathbf{Z}_n^{\text{P}} - \widehat{\mathbf{v}}_i)^{\text{T}}(A_i^{-1} + \sigma_{\text{P}}^2 I)^{-1}(\mathbf{Z}_n^{\text{P}} - \widehat{\mathbf{v}}_i)\right), \quad (13)$$

where

$$\widehat{C}_i := \exp\left(-\frac{1}{2} \log \det K_i - \frac{M}{2} \log 2\pi - M \log \sigma_{\text{P}} + Q(\widehat{\mathbf{v}}_i) - \frac{1}{2} \log \det(A_i + \sigma_{\text{P}}^{-2} I)\right).$$

*Proof.* See Appendix C. □

Consequently, the test statistic (8) is approximated by

$$\begin{aligned} -\log \widehat{\Lambda}(\mathbf{Z}_n^{\text{P}}) &= -\log \widehat{p}(\mathbf{Z}_n^{\text{P}}|\mathcal{H}_0) + \log \widehat{p}(\mathbf{Z}_n^{\text{P}}|\mathcal{H}_1) \\ &= \frac{1}{2} \left( \log \det(A_0 + \sigma_{\text{P}}^{-2} I) + \log \det K_0 - 2Q(\widehat{\mathbf{v}}_0) - \log \det(A_1 + \sigma_{\text{P}}^{-2} I) \right. \\ &\quad \left. - \log \det K_1 + 2Q(\widehat{\mathbf{v}}_1) \right) + \frac{1}{2} (\mathbf{Z}_n^{\text{P}} - \widehat{\mathbf{v}}_0)^{\text{T}} (A_0^{-1} + \sigma_{\text{P}}^2 I)^{-1} (\mathbf{Z}_n^{\text{P}} - \widehat{\mathbf{v}}_0) \\ &\quad - \frac{1}{2} (\mathbf{Z}_n^{\text{P}} - \widehat{\mathbf{v}}_1)^{\text{T}} (A_1^{-1} + \sigma_{\text{P}}^2 I)^{-1} (\mathbf{Z}_n^{\text{P}} - \widehat{\mathbf{v}}_1). \end{aligned} \quad (14)$$

We use  $-\log \widehat{\Lambda}(\mathbf{Z}_n^{\text{P}})$  as the test statistic in the WGPLRT and reject  $\mathcal{H}_0$  if  $-\log \widehat{\Lambda}(\mathbf{Z}_n^{\text{P}}) > -\log \gamma^{\text{P}}$ . The test procedure is summarized in Algorithm 1.

**Remark 8.** *The Laplace approximation in Proposition 7 may perform poorly when  $\text{range}(W_i) \neq \mathbb{R}$  unless the distance between  $\widehat{\mathbf{v}}_i$  and the boundary of  $(\text{range}(W_i))^M$  is large relative to  $\sigma_{\text{P}}$ . Moreover, since the Laplace approximation captures only the local characteristics of the integrand in (9) around its maximum, WGPLRT sometimes approximates the LRT poorly when the only difference between  $\mathcal{H}_0$  and  $\mathcal{H}_1$  lies in the tails of the warping distributions.*

We have now acquired the analytic expression of the approximated test statistic in the WGPLRT for point observations. We devote the next subsection to studying the case of integral observations.

---

**Algorithm 1:** Warped Gaussian Process Likelihood Ratio Test (WGPLRT)

---

**Input:** the point observations  $\mathbf{Z}_n^P$  at  $n$ -th P-sensor, the covariance matrix  $K_i$  defined as in Proposition 6 and the warping function  $W_i$  for  $i = 0, 1$ , the noise variance  $\sigma_P^2 > 0$ , and the test threshold  $\gamma^P$ .

**Output:** the log-approximated test statistic  $-\log \widehat{\Lambda}(\mathbf{Z}_n^P)$  and the binary decision  $\widehat{y}_n^P$  at  $\mathbf{x}_n^P$ .

- 1 Compute  $\widehat{\mathbf{v}}_i = \arg \max_{\mathbf{v}} Q_i(\mathbf{v})$  and  $A_i = -\nabla^2 Q_i(\mathbf{v})|_{\mathbf{v}=\widehat{\mathbf{v}}_i}$  for  $i = 0, 1$ .
- 2 Compute  $\widehat{p}(\mathbf{Z}_n^P | \mathcal{H}_i)$  for  $i = 0, 1$  using (12) in Proposition 7.
- 3 Compute  $-\log \widehat{\Lambda}(\mathbf{Z}_n^P)$  using (14). The decision  $\widehat{y}_n^P$  is given by

$$\widehat{y}_n^P = \begin{cases} 1, & \text{if } -\log \widehat{\Lambda}(\mathbf{Z}_n^P) > -\log \gamma^P \\ 0, & \text{if } -\log \widehat{\Lambda}(\mathbf{Z}_n^P) \leq -\log \gamma^P. \end{cases}$$


---

### B. Local binary decisions for integral observations

We now derive the algorithm called **Neighborhood-density-based Likelihood Ratio Test (NLRT)** for making local binary decisions at the Integral sensors. In summary, NLRT generates samples under both  $\mathcal{H}_0$  and  $\mathcal{H}_1$  and assigns the observation to the “nearest” hypothesis, where the notion of distance is defined later. To begin with, for  $i = 0, 1$ , we are again interested in the marginal likelihood  $p(\mathbf{Z}_n^I | \mathcal{H}_i)$ , which is given by

$$p(\mathbf{Z}_n^I | \mathcal{H}_i) = \int_{\mathbb{R}^K} p(\mathbf{Z}_n^I | \tilde{\mathbf{Z}}_n^I) p(\tilde{\mathbf{Z}}_n^I | \mathcal{H}_i) d\tilde{\mathbf{Z}}_n^I. \quad (15)$$

Note that  $\mathbf{Z}_n^I | \tilde{\mathbf{Z}}_n^I \sim \mathcal{N}(\tilde{\mathbf{Z}}_n^I, \sigma_I^2 \mathbf{I}_K)$ . Unfortunately, the marginal likelihood in (15) is also computationally intractable as the observations  $\mathbf{Z}_n^I$  are defined by integrals. To overcome this problem, we propose the NLRT, which is based on the idea of the Approximate Bayesian Computation method (see, e.g., [31, Section 2.1]).

In NLRT, we generate samples under  $\mathcal{H}_0$  and  $\mathcal{H}_1$  and accept each sample if it is within a certain error tolerance  $\delta^I > 0$  to the given observation. Subsequently, the test statistic (8) is approximated by the ratio of the number of accepted samples under  $\mathcal{H}_0$  and  $\mathcal{H}_1$ ; see details in Algorithm 2. To measure the distances between the generated samples and the observations, the Euclidean distance is a natural yet effective candidate in most cases. However, for high-dimensional data, the Euclidean distance fails to define a meaningful notion of proximity as shown in Theorem 1

in [2]. Therefore, summary statistics are required to project high-dimensional data to a low-dimensional space while preserving their distinct characteristics under  $\mathcal{H}_0$  and  $\mathcal{H}_1$ . In our case, depending on the type of the hypotheses, feature-engineering is needed for designing summary statistics: mode, mean, variance, kurtosis can be used to capture the differences in the warping distributions; and autocorrelation (ACF) is helpful to detect the differences between covariance functions  $\mathcal{C}_0$  and  $\mathcal{C}_1$ .

---

**Algorithm 2:** Neighborhood-density-based Likelihood Ratio Test (NLRT)

---

**Input:** the integral observations  $\mathbf{Z}_n^I$  at  $n$ -th I-sensor, the number of generated samples  $J$ , the warping functions  $W_i$  and the covariance functions  $\mathcal{C}_i(\cdot, \cdot)$  for  $i = 0, 1$ , the summary statistic  $S : \mathbb{R}^K \rightarrow \mathbb{R}^l$  for some  $l \in \mathbb{N}$  with  $l < K$ , the distance measure  $d(\cdot, \cdot) : \mathbb{R}^l \times \mathbb{R}^l \rightarrow \mathbb{R}$ , the noise variance  $\sigma_1^2 > 0$ , the error tolerance  $\delta^I > 0$ , some  $\epsilon^I > 0$  small enough, and the test threshold  $\gamma^I$ .

**Output:** the approximated test statistic  $\widehat{\Lambda}(\mathbf{Z}_n^I)$  and the decision  $\widehat{y}_n^I$  at  $\mathbf{x}_N^I$ .

- 1 For  $i = 0, 1$  and  $j = 1, \dots, J$ , generate samples  $\widehat{\mathbf{Z}}_j^{I,i}$  according to (SN3).
- 2 For  $i = 0, 1$  and  $j = 1, \dots, J$ , accept  $\widehat{\mathbf{Z}}_j^{I,i}$  if

$$d(S(\mathbf{Z}_n^I), S(\widehat{\mathbf{Z}}_j^{I,i})) \leq \delta^I.$$

- 3 For  $i = 0, 1$ , denote the number of accepted samples as  $n_{\mathcal{H}_i}$ . Compute the approximated test statistic

$$\widehat{\Lambda}(\mathbf{Z}_n^I) = \frac{n_{\mathcal{H}_0} + \epsilon^I}{n_{\mathcal{H}_1} + \epsilon^I}.$$

- 4 The decision  $\widehat{y}_n^I$  is given by

$$\widehat{y}_n^I = \begin{cases} 1, & \text{if } \widehat{\Lambda}(\mathbf{Z}_n^I) < \gamma^I \\ 0, & \text{if } \widehat{\Lambda}(\mathbf{Z}_n^I) \geq \gamma^I. \end{cases}$$


---

**Remark 9.** *The Laplace Approximation technique does not work for the integral case as the marginal likelihood  $p(\mathbf{Z}_n^I | \mathcal{H}_i)$  for  $i = 0, 1$  cannot be expressed analytically.*

**Remark 10.** *A small positive number  $\epsilon^I$  is added in Line 3 of Algorithm 2 when evaluating the approximated test statistic to avoid division by zero.*

## V. STEP 2: SPATIAL BEST LINEAR UNBIASED ESTIMATOR (S-BLUE)

Given the collection of binary decisions  $\widehat{\mathbf{Y}}_{1:N} := (\widehat{y}_1^P, \dots, \widehat{y}_{N^P}^P, \widehat{y}_1^I, \dots, \widehat{y}_{N^I}^I)^\top$  at all  $N$  sensors, we aim to derive the **Spatial Best Linear Unbiased Estimator (S-BLUE)**  $\widehat{g}_*$  for  $g_* := g(\mathbf{x}_*)$  for a fixed un-monitored spatial location  $\mathbf{x}_* \in \mathcal{X}$ . Then, the prediction of  $y_* := y(\mathbf{x}_*)$  is given by

$$\widehat{y}_* = \mathbb{1}_{\{\widehat{g}_* \geq c\}}. \quad (16)$$

Let  $l : \mathbb{R} \times \mathbb{R} \rightarrow \mathbb{R}_+$  denote the loss function. Let  $\mathcal{R}[h]$  denote the Bayes risk of any  $h : \mathbb{R}^N \rightarrow \mathbb{R}$ , that is

$$\mathcal{R}[h] = \mathbb{E}[l(h(\widehat{\mathbf{Y}}_{1:N}), g_*)]. \quad (17)$$

We restrain the estimator to be a member of the family of linear estimators,  $\mathcal{H} := \{h : \mathbb{R}^N \rightarrow \mathbb{R} : h(\widehat{\mathbf{Y}}_{1:N}) = \mathbf{w}^\top \widehat{\mathbf{Y}}_{1:N} + b, \mathbf{w} \in \mathbb{R}^N, b \in \mathbb{R}\}$ , where  $\mathbf{w}$  is called a weight vector,  $b$  is called an intercept, and neither is a function of  $\widehat{\mathbf{Y}}_{1:N}$ . The S-BLUE is defined to be the optimal linear estimator minimizing the Bayes risk under the quadratic loss function defined by

$$\widehat{h}_{\text{S-BLUE}} := \arg \min_{h \in \mathcal{H}} \mathbb{E}[(h(\widehat{\mathbf{Y}}_{1:N}) - g_*)^2]. \quad (18)$$

Let us re-index  $(\mathbf{x}_1^P, \dots, \mathbf{x}_{N^P}^P, \mathbf{x}_1^I, \dots, \mathbf{x}_{N^I}^I)$  as  $(\mathbf{x}_1, \dots, \mathbf{x}_N)$  and re-index  $\widehat{\mathbf{Y}}_{1:N}$  as  $(\widehat{y}_1, \dots, \widehat{y}_N)^\top$ . Observe that the binary decision  $\widehat{y}_n$  at location  $\mathbf{x}_n$  from the Likelihood Ratio Test is an estimator of the ground-truth  $y_n$  with type I and type II errors. Therefore, the effect of the Likelihood Ratio Test at each  $\mathbf{x}_n$  can be treated as applying a transition matrix that adds noise to the true label during data transmission, as detailed in the following Remark.

**Remark 11.** For  $n = 1, \dots, N$ , let  $\gamma^n \in \{\gamma^P, \gamma^I\}$  denote the test threshold for the Likelihood Ratio Test (either WGPLRT or NLRT) at  $\mathbf{x}_n$ , then the effect of the Likelihood Ratio Test at  $\mathbf{x}_n$  is equivalent to transmitting the ground-truth  $y(\mathbf{x}_n)$  via a noisy channel, where the transition matrix  $U_n$  is given by

$$U_n = \begin{matrix} & \begin{matrix} 0 & 1 \end{matrix} \\ \begin{matrix} 0 \\ 1 \end{matrix} & \begin{pmatrix} p_{00}^n & p_{01}^n \\ p_{10}^n & p_{11}^n \end{pmatrix}, \end{matrix} \quad (19)$$

where  $p_{01}^n := \mathbb{P}[\widehat{\Lambda} < \gamma^n | \mathcal{H}_0]$  is the type I error rate,  $p_{00}^n := 1 - p_{01}^n$ ,  $p_{10}^n := \mathbb{P}[\widehat{\Lambda} \geq \gamma^n | \mathcal{H}_1]$  is the type II error rate, and  $p_{11}^n := 1 - p_{10}^n$ .

Therefore, the system model now can be partitioned into two disjoint layers: the first layer for the Likelihood Ratio Tests (LRTs) and the second layer for the Spatial BLUE (S-BLUE) with noisy inputs. The S-BLUE is presented in the following theorem.

**Theorem 12** (Spatial BLUE).

Given the binary decisions  $\widehat{\mathbf{Y}}_{1:N} = (\widehat{y}_1, \dots, \widehat{y}_N)^\top$  obtained in Algorithm 1 & 2 and the transition matrices  $\{U_n\}_{n=1}^N$  specified in (19), the S-BLUE of  $g_* = g(\mathbf{x}_*)$  for a fixed un-monitored location  $\mathbf{x}_* \in \mathcal{X}$  is given by

$$\widehat{g}_* := \widehat{h}_{S-BLUE}(\widehat{\mathbf{Y}}_{1:N}) = \mu_* + \text{Cov}[g_*, \widehat{\mathbf{Y}}_{1:N}] \text{Cov}[\widehat{\mathbf{Y}}_{1:N}]^{-1} (\widehat{\mathbf{Y}}_{1:N} - \mathbb{E}[\widehat{\mathbf{Y}}_{1:N}]), \quad (20)$$

where  $\mu_* := \mathbb{E}[g_*]$ , and for  $i, j = 1, \dots, N$ ,

$$\mathbb{E}[\widehat{y}_i] = p_{11}^i \Phi\left(-\frac{c - \mu_i}{\sigma_i}\right) + p_{01}^i \Phi\left(\frac{c - \mu_i}{\sigma_i}\right),$$

$$\begin{aligned} \text{Cov}[\widehat{y}_i, \widehat{y}_j] &= p_{01}^i p_{01}^j \mathbb{P}(g_i < c, g_j < c) + p_{01}^i p_{11}^j \mathbb{P}(g_i < c, g_j \geq c) \\ &\quad + p_{11}^i p_{01}^j \mathbb{P}(g_i \geq c, g_j < c) + p_{11}^i p_{11}^j \mathbb{P}(g_i \geq c, g_j \geq c) \\ &\quad - \left[ p_{11}^i \Phi\left(-\frac{c - \mu_i}{\sigma_i}\right) + p_{01}^i \Phi\left(\frac{c - \mu_i}{\sigma_i}\right) \right] \left[ p_{11}^j \Phi\left(-\frac{c - \mu_j}{\sigma_j}\right) + p_{01}^j \Phi\left(\frac{c - \mu_j}{\sigma_j}\right) \right], \\ \text{Cov}[g_*, \widehat{y}_i] &= \frac{1}{\sqrt{2\pi}\sigma_i} (p_{11}^i - p_{01}^i) \mathcal{C}(\mathbf{x}_*, \mathbf{x}_i) \exp\left(-\frac{(c - \mu_i)^2}{2\sigma_i^2}\right). \end{aligned} \quad (21)$$

with  $g_i := g(\mathbf{x}_i)$ ,  $\mu_i := \mu(\mathbf{x}_i)$ ,  $\sigma_i^2 := \mathcal{C}(\mathbf{x}_i, \mathbf{x}_i)$ , and  $c$  is the constant threshold in (2).

*Proof.* See Appendix D. □

**Remark 13.** For  $i, j = 1, \dots, N$ , as  $(g_i, g_j)^\top \sim \mathcal{N}\left(\begin{pmatrix} \mu_i \\ \mu_j \end{pmatrix}, \begin{pmatrix} \sigma_i^2 & \mathcal{C}(\mathbf{x}_i, \mathbf{x}_j) \\ \mathcal{C}(\mathbf{x}_i, \mathbf{x}_j) & \sigma_j^2 \end{pmatrix}\right)$ ,  $\mathbb{P}(g_i < c, g_j < c)$ ,  $\mathbb{P}(g_i < c, g_j \geq c)$ ,  $\mathbb{P}(g_i \geq c, g_j < c)$ ,  $\mathbb{P}(g_i \geq c, g_j \geq c)$  are the probability of the bivariate normal over the regions  $(-\infty, c) \times (-\infty, c)$ ,  $(-\infty, c) \times [c, \infty)$ ,  $[c, \infty) \times (-\infty, c)$ ,  $[c, \infty) \times [c, \infty)$ , respectively.

As a consequence, the theoretical Bayes risk can be computed analytically as shown in the following Corollary.

**Corollary 14** (Bayes risk).

Under the quadratic loss function, the Bayes risk (17) associated with  $\widehat{h}_{S-BLUE}(\widehat{\mathbf{Y}}_{1:N})$  defined

---

**Algorithm 3:** Classification of binary spatial random field
 

---

**Input:** the binary decisions  $\widehat{\mathbf{Y}}_{1:N}$ , the transition matrices  $\{U_n\}_{n=1}^N$ , the constant threshold  $c$ , the mean function  $\mu(\cdot)$ , the covariance function  $\mathcal{C}(\cdot, \cdot)$ , the un-monitored location  $\mathbf{x}_*$ .

**Output:** the prediction  $\widehat{y}_*$  at  $\mathbf{x}_*$  and the Bayes risk  $\mathcal{R}[\widehat{h}_{\text{S-BLUE}}(\widehat{\mathbf{Y}}_{1:N})]$ .

1 **Offline phase:** Compute  $\mu_*$ ,  $\text{Cov}[g_*, \widehat{\mathbf{Y}}_{1:N}]$ ,  $\text{Cov}[\widehat{\mathbf{Y}}_{1:N}]$ ,  $\mathbb{E}[\widehat{\mathbf{Y}}_{1:N}]$  using (21).

2 **Online Phase:** After collecting the decisions  $\widehat{\mathbf{Y}}_{1:N}$ , compute

$$\widehat{g}_* = \widehat{h}_{\text{S-BLUE}}(\widehat{\mathbf{Y}}_{1:N}) = \mu_* + \text{Cov}[g_*, \widehat{\mathbf{Y}}_{1:N}] \text{Cov}[\widehat{\mathbf{Y}}_{1:N}]^{-1} (\widehat{\mathbf{Y}}_{1:N} - \mathbb{E}[\widehat{\mathbf{Y}}_{1:N}]).$$

3 Compute  $\widehat{y}_* = \mathbb{1}_{\{\widehat{g}_* \geq c\}}$ .

4 Compute  $\mathcal{R}[\widehat{h}_{\text{S-BLUE}}(\widehat{\mathbf{Y}}_{1:N})]$  using (22).

---

in (20) is given by

$$\mathcal{R}[\widehat{h}_{\text{S-BLUE}}(\widehat{\mathbf{Y}}_{1:N})] = \text{Cov}[g_*] - \text{Cov}[g_*, \widehat{\mathbf{Y}}_{1:N}] \text{Cov}[\widehat{\mathbf{Y}}_{1:N}]^{-1} \text{Cov}[g_*, \widehat{\mathbf{Y}}_{1:N}]^T. \quad (22)$$

*Proof.* See Appendix E. □

We may execute the S-BLUE algorithm via two stages: the first is the **offline stage** where we compute the quantities such as  $\mathbb{E}[\widehat{y}_i]$ ,  $\text{Cov}[\widehat{y}_i, \widehat{y}_j]$ ,  $\text{Cov}[g_*, \widehat{y}_i]$ , and store their values; then, during the **online stage**, given the decisions  $\widehat{\mathbf{Y}}_{1:N}$ , we may compute the estimator  $\widehat{g}_*$  using (20). This procedure is presented in the Algorithm 3.

After formulating the S-BLUE, the overall algorithm is outlined in Algorithm 4.

## VI. EXPERIMENTS WITH SYNTHETIC DATA

We conduct two experiments with synthetic data to study the performance of the proposed methods in Algorithm 4. Section VI-A demonstrates the ability of our proposed method to reconstruct the binary spatial random field. In Section VI-B, we perform a sensitivity analysis on the two LRT algorithms when the noise variance and the number of observations vary. To simplify the nomenclature, from now on, we say a process is warped by a random variable when the warping function is of the form  $W = F^{-1} \circ \Phi$ , where  $F$  is the CDF of that random variable.

The proposed algorithm is compared to two algorithms: the ‘‘oracle’’, in which the values of the latent GP  $g$  that generates the binary spatial field at the sensor locations are known and the field is reconstructed via Gaussian Process Regression; and the K-Nearest Neighbors (KNN)

---

**Algorithm 4:** The Overall Algorithm
 

---

**Input:** the observations  $(\mathbf{Z}_{1:N^P}^P, \mathbf{Z}_{1:N^I}^I)$ , the time points  $T_{1:M}^P$ , the time intervals  $T_{1:K}^I$ , the test threshold  $\gamma^j$  for the Likelihood Ratio Test and the noise variance  $\sigma_j^2 > 0$  for  $j \in \{I, P\}$ , the covariance function  $\mathcal{C}_i(\cdot, \cdot)$  and the warping function  $W_i$  for the temporal processes for  $i = 0, 1$ , the summary statistic  $S(\cdot)$ , the distance measure  $d(\cdot, \cdot)$ , the number of generated samples  $J$ , the error tolerance  $\delta^I > 0$ , some  $\epsilon^I > 0$  small enough, the mean function  $\mu(\cdot)$  and the covariance function  $\mathcal{C}(\cdot, \cdot)$  for the binary spatial field, the transition matrices  $\{U_n\}_{n=1}^N$ , the constant threshold  $c$ , the un-monitored location  $\mathbf{x}_*$ .

**Output:** the prediction  $\hat{y}_*$  at  $\mathbf{x}_*$  and the Bayes risk  $\mathcal{R}[\hat{h}_{\text{S-BLUE}}(\hat{\mathbf{Y}}_{1:N})]$ .

- 1 Compute  $K_i = \mathcal{C}_i(T_{1:M}^P, T_{1:M}^P)$  by definition for  $i = 0, 1$ .
  - 2 For  $j = 1, \dots, N^P$ , compute  $\hat{y}_j^P$  using Algorithm 1.
  - 3 For  $j = 1, \dots, N^I$ , compute  $\hat{y}_j^I$  using Algorithm 2.
  - 4 Compute  $\hat{y}_*$  and  $\mathcal{R}[\hat{h}_{\text{S-BLUE}}(\hat{\mathbf{Y}}_{1:N})]$  using Algorithm 3.
- 

algorithm, in which given the noisy predictions  $\hat{\mathbf{Y}}_{1:N}$  from the sensors, the KNN classifier will assign an un-monitored spatial location  $\mathbf{x}_*$  to a class, i.e.,  $y(\mathbf{x}_*) = 1$  or  $y(\mathbf{x}_*) = 0$ , based on a plurality vote among the  $k$  nearest neighbors of  $\mathbf{x}_*$ . The optimal distance metric as well as the value of  $k$  for the KNN are obtained by cross-validation techniques.

#### A. Experiment 1: Evaluation on the Synthetic Dataset – Spatial Field Reconstruction

We first examine the ability of the proposed methods to reconstruct the binary spatial random field using a synthetic dataset. We create a synthetic dataset of sensor network deployed over  $[-5, 5] \times [-5, 5] \subset \mathbb{R}^2$  with  $50 \times 50$  spatial locations spaced evenly across the region. The latent spatial random field  $g$  is modeled using a GP with mean 0 and the Squared Exponential covariance function  $\mathcal{C}_{l_g, s_g}(\cdot, \cdot)$  (see, e.g., [26, Section 4.2.1]), where the length-scale  $l_g = 1/2$  and the scale  $s_g = 1$ , i.e.,

$$\mathcal{C}(\mathbf{x}, \mathbf{x}') = s_g^2 \exp\left(-\frac{(\mathbf{x} - \mathbf{x}')^\top (\mathbf{x} - \mathbf{x}')}{2l_g^2}\right).$$

The process is then warped by a Bernoulli( $\pi$ ), where  $\pi = 0.5$ , i.e.,  $c = \Phi^{-1}(1 - \pi) = 0$  (see details in Remark 3), to generate the binary spatial field  $y$ .

At each spatial location  $\mathbf{x}$ , based on the value  $y(\mathbf{x})$  of the binary spatial field, a temporal process  $f(\cdot; \mathbf{x})$  is generated according to (TP1), where the corresponding covariance functions  $\mathcal{C}_0, \mathcal{C}_1$  are the Matérn covariance functions (see, e.g., [26, Section 4.2.1]) with  $\nu = 1/2, 5/2$ , respectively. That is, for any  $t, t' \in [0, T]$ , we have

$$\mathcal{C}_0(t, t') = s_f^2 \exp\left(-\frac{r}{l_f}\right), \quad (23)$$

$$\mathcal{C}_1(t, t') = s_f^2 \left(1 + \frac{\sqrt{5}r}{l_f} + \frac{5r^2}{3l_f^2}\right) \exp\left(-\sqrt{5}\frac{r}{l_f}\right), \quad (24)$$

where the signal variance  $s_f^2 = 1$ , the length-scale  $l_f = 1$ , and  $r := |t - t'|$  is the distance between  $t$  and  $t'$ .

In either case, the temporal process is warped by a random variable following Tukey's  $g$ -and- $h(g, h, l, s)$  distribution where  $g = 0.1, h = 0.4, l = 1$ , and  $s = 1$ ; see, e.g., [36]. Note that a random variable  $Y$  follows  $g$ -and- $h(g, h, l, s)$  if

$$Y = l + s \left( \frac{\exp(gZ) - 1}{g} \right) \exp(hZ^2),$$

where  $Z \sim \mathcal{N}(0, 1)$  is a standard normal random variable.

Out of the 2500 spatial locations, 250 randomly chosen spatial locations are monitored by the sensors, half of which are P-sensors and the other half are I-sensors (see Figure (2a) for the true binary spatial random field). The P-sensors collect point observations at 50 time points equally spaced over  $[0, 20]$ . Similarly, the I-sensors collect integral observations over the 50 consecutive time intervals of equal length over  $[0, 20]$ . Our interest is to reconstruct the values of the binary spatial field at the remaining 2250 un-monitored locations from the point and integral observations  $(\mathbf{Z}_{1:N^P}^P, \mathbf{Z}_{1:N^I}^I)$  collected from the sensors.

When all the Point and Integral sensors have the noise standard deviation  $\sigma_I = \sigma_P = 0.1$ , the LRT thresholds are set to  $\gamma^P = \exp(178.1392)$  and  $\gamma^I = \exp(-0.4659)$ , such that the False Positive Rate (FPR) of each sensor is controlled by a significance level  $\alpha = 0.1$ . For NLRT, the summary statistics are autocorrelations (ACF) with lags 1 to 4 (see, e.g., [3, Section 2.1]), the distance measure is the Euclidean distance, the error tolerance is  $\delta^I = 0.1, \epsilon^I = 0.1$ , and the number of generated samples is set to  $J = 10000$ . Finally, at each sensor location, we set the transition matrix (see (19)) to either

$$U^P = \begin{pmatrix} 0.8938 & 0.1062 \\ 0.1684 & 0.8316 \end{pmatrix} \quad \text{or} \quad U^I = \begin{pmatrix} 0.8962 & 0.1038 \\ 0.1468 & 0.8532 \end{pmatrix}$$

depending on the sensor type. The test thresholds  $\gamma^P, \gamma^I$  and the transition matrices  $U^P, U^I$  are computed via simulation beforehand, where we estimate the CDFs of the approximated test statistics under  $\mathcal{H}_0$  and  $\mathcal{H}_1$  using Monte-Carlo methods.

Under the parameters specified above, Figure (2a) and (2b) show the true binary spatial field and the reconstructed binary spatial field, respectively. The averaged mean-square-error (MSE), F1 score, false positive rate (FPR), and true positive rate (TPR) over 100 realizations of the oracle, our proposed method (S-BLUE), and the KNN is presented in Table II. Overall, we observe that our proposed method outperforms KNN and achieves slightly worse results compared with the oracle.

To further study the impacts of the noise variance when observing the temporal processes, we plot the averaged MSE, F1 score, FPR, and TPR over 20 realizations against the noise variance of Algorithm 4 in Figure (2c). Again, we assume  $\sigma_I = \sigma_P$  for simplicity. The test thresholds and transition matrices are computed via simulation beforehand for each value of the noise variance. When the noise variance becomes smaller, observe that the FPR stays relatively constant because the significance level is controlled to be around 0.1. In contrast, notice that the TPR increases, which leads to an improvement in the F1 score and MSE.

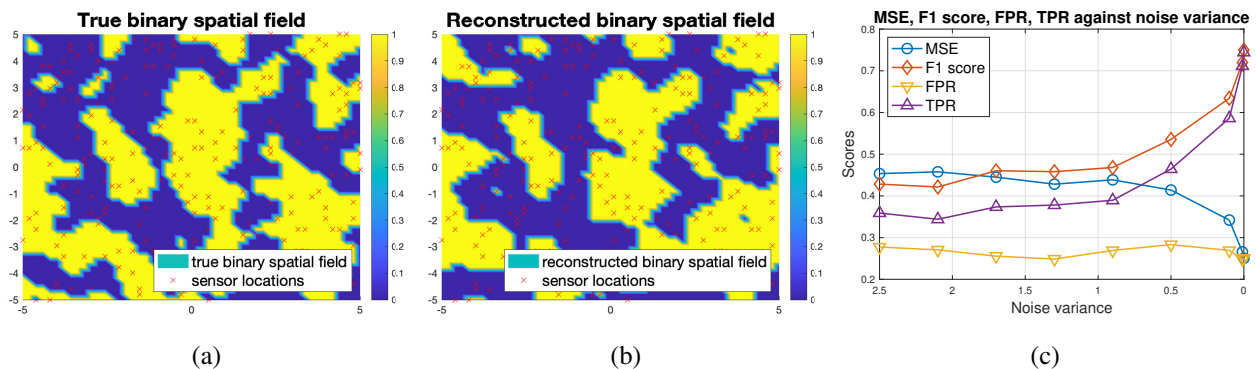


Figure 2: Experiment 1 – Figure (2a) is the true binary spatial field, where the crosses denote the spatial locations of the sensors. Figure (2b) is the reconstructed binary spatial field from our algorithm. Figure (2c) shows the averaged MSE, F1 score, FPR, and TPR over 20 realizations against the noise variance.

Algorithm	MSE	F1 score	FPR	TPR
Oracle	0.1207	0.8775	0.1191	0.8757
S-BLUE	0.2632	0.7292	0.2502	0.7202
KNN	0.3141	0.6630	0.2710	0.6334

Table II: Experiment 1 – Averaged MSE, F1 score, FPR, TPR over 100 realizations.

### B. Experiment 2 : Evaluation on the Synthetic Dataset – Sensitivity Analysis on LRTs

In the second experiment, we perform a sensitivity analysis on the two LRT algorithms by varying the number of observations as well as the noise variance. We aim to differentiate between the same hypotheses defined in (23) and (24). Except for the number of observations and the noise variance, all other parameters in the two LRTs are set up as in the Subsection VI-A. In Figure (3a), we fix  $\sigma_I = 0.1$  and study the effect of the number of integral observations on the Receiver Operating Characteristic (ROC) curves of NLRT by evaluating the Area Under Curve (AUC). We note that AUC reaches its peak when  $K = 64$ , indicating that the performance of NLRT first improves then deteriorates when  $K$  varies from 10 to 130. This result arises because the length of time intervals where the integrals are taken is reduced when the number of integral observations increases. Consequently, the power of the signal wanes, which leads to less accurate integral observations. In contrast, when the noise variance is much smaller, e.g.,  $\sigma_I = 0.01$ , we observe that the AUC does not decrease as the number of integral observations increases. However, such phenomenon is not observed for WGPLRT since the distributions of point observations do not change when the number of point observations increases. Figure (3b) compares the ROC curves between WGPLRT for the P-sensors and NLRT for the I-sensors when the number of observations are  $M = K = 64$ , at which the performance of NLRT is the best. The figure suggests that when the FPR is smaller than approximately 0.1, WGPLRT performs better than NLRT. While if the FPR exceeds approximately 0.1, both algorithms have comparable performance. This fact offers a reference for practitioners to choose the type of sensors for deployment that minimizes the total deployment costs while keeping a reasonable performance of the model. Finally, we study the effect of the noise variance on both WGPLRT and NLRT in Figure (3c) when the number of observations is again set to be  $M = K = 64$ . Unsurprisingly, the AUC of both WGPLRT and NLRT increase as the noise variance decreases.

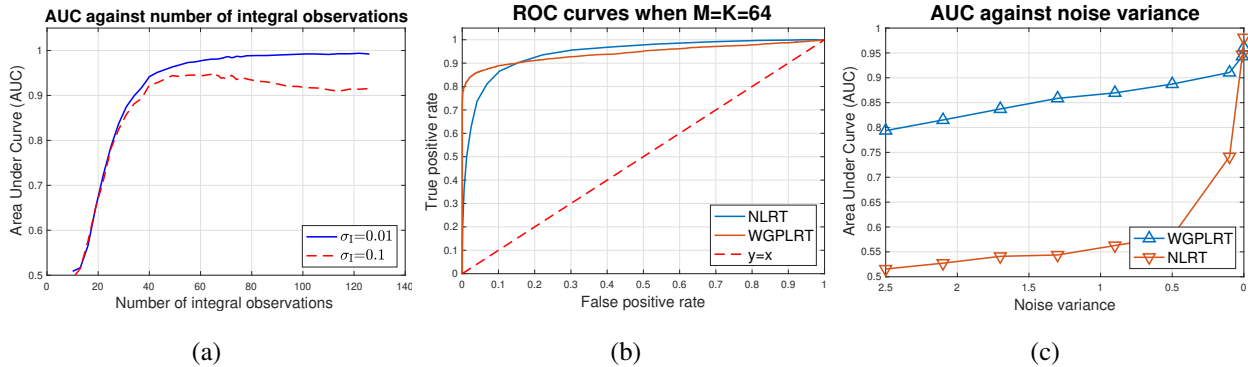


Figure 3: Experiment 2 – Figure (3a) shows the effect of the number of integral observations on the AUC of NLRT. Figure (3b) compares the ROC curves of WGPLRT and NLRT when the number of observations are  $M = K = 64$ . Figure (3c) shows the AUC of WGPLRT and NLRT against the noise variance when  $M = K = 64$ .

## VII. EVALUATION ON THE REAL DATASET

In the real-world experiments, we study a weather dataset<sup>4</sup> from the National Environment Agency (NEA) of Singapore. The dataset contains hourly measurements of Temperature, Wet Bulb Temperature, Dew Point Temperature, Scalar Mean Wind Direction, Relative Humidity, Scalar Mean Wind Speed, and Sea-Level Pressure at 21 weather stations. The measurements are mainly between 2010 to 2018, yet their starting dates and ending dates vary depending on the stations. Among the 21 stations, 5 stations (with station number S06, S23, S24, S25, S80) are installed as early as 2005 and they also take hourly measurements of Total Rainfall and Cloud Cover. The spatial locations of the weather stations are visualized in Figure (7a).

In this section, we aim to synthetically generate sensor observations based on the dataset and reconstruct the binary spatial random field at other spatial locations over Singapore where no weather stations are deployed.

### A. Data Preprocessing

To begin with, we observe that some weather stations only take measurements between 5:00 a.m. to 23:00 p.m., hence all measurements outside this period are removed for consistency. Furthermore, to reduce seasonal variation, we take data over 17 weeks during the Southwest

<sup>4</sup><https://data.gov.sg/search?groups=environment>, retrieved on 7 January 2022.

Monsoon Season<sup>5</sup> in 2012, i.e., from 03/06/2012 (Sunday) to 29/09/2012 (Saturday). Next, we select the fields of interest to represent the binary spatial random field and the temporal processes. For the binary spatial random field, we take the average weekly relative humidity as the latent GP and the constant threshold  $c$  is taken to be the median of all data. Figure 4 shows the histogram and Q-Q plot of the average weekly relative humidity. Observe that the normality assumption holds. For the temporal processes, hourly measurements of temperature are used. For each hour from 5:00 a.m. to 23:00 p.m., the average hourly temperature over all weather stations is subtracted from the measurements to center the measurements. The processed measurements are named as *centered temperatures (CT)*. Then, they are further partitioned into two subsets based on the level of the average weekly relative humidity (i.e., over or below the constant threshold  $c$ ) to represent the temporal processes under  $\mathcal{H}_0$  and  $\mathcal{H}_1$ . Figure 5 shows the density plots of the centered temperatures from the two subsets. We notice that the data are left-skewed and the transformed data under  $x \mapsto 10 - x$  can be modeled using Gamma distributions for suitable hyperparameters fitted from data; see also Table IV. Figure 6 presents the Q-Q plots of the transformed data from the two subsets against the fitted Gamma distributions, respectively.

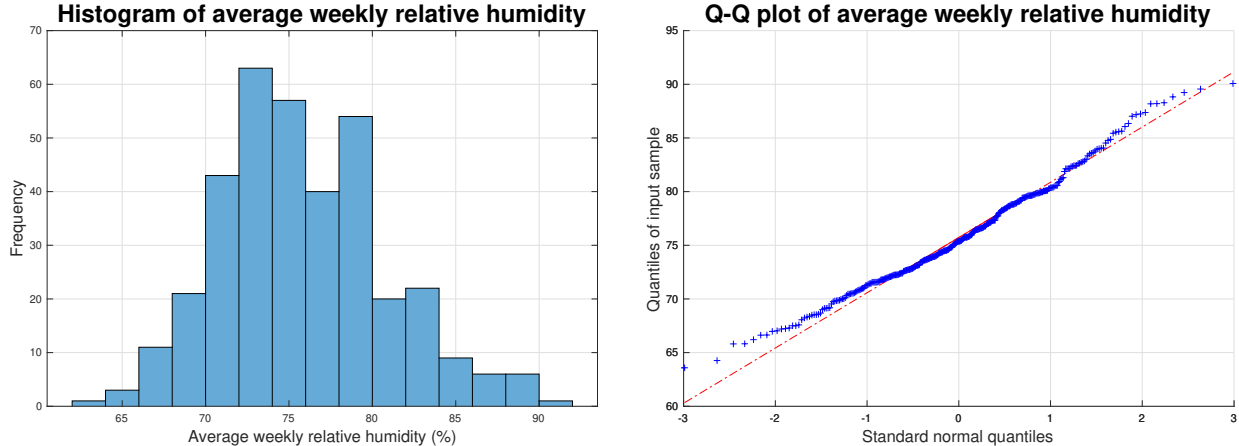


Figure 4: Real-world experiment – Histogram and normal Q-Q plot of the average weekly relative humidity.

<sup>5</sup>See details in <http://www.weather.gov.sg/climate-climate-of-singapore>.

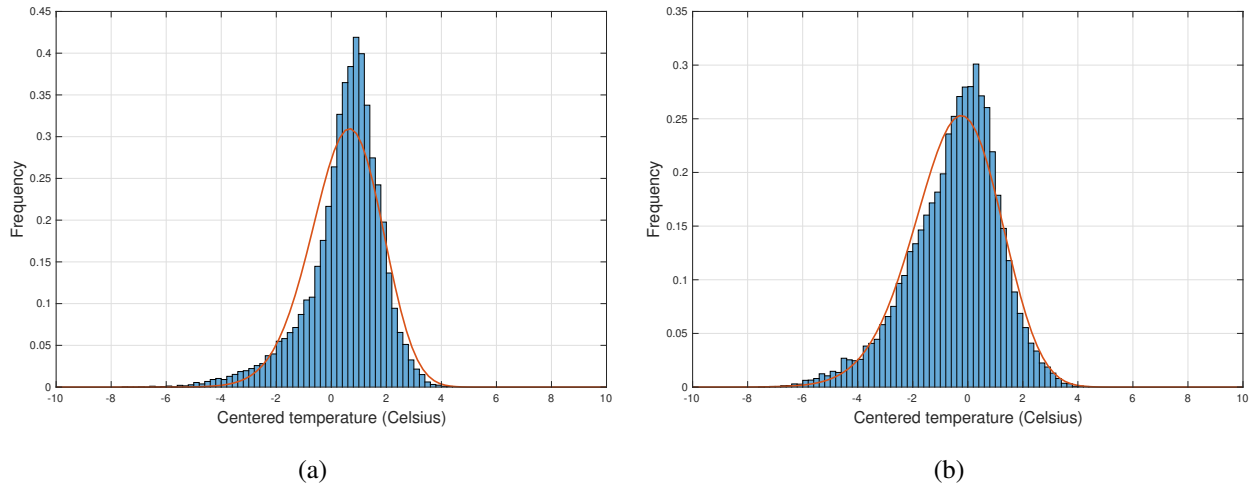


Figure 5: Real-world experiment – Figure (5a) shows the density plot of the centered temperatures when the average weekly relative humidity is below the constant threshold  $c$ . Figure (5b) shows the histogram of the centered temperatures when the average weekly relative humidity is above the constant threshold  $c$ . The orange-colored curves in both Figure (5a) and Figure (5b) indicate the flipped and shifted graphs of the probability density functions of the fitted Gamma distributions, respectively.

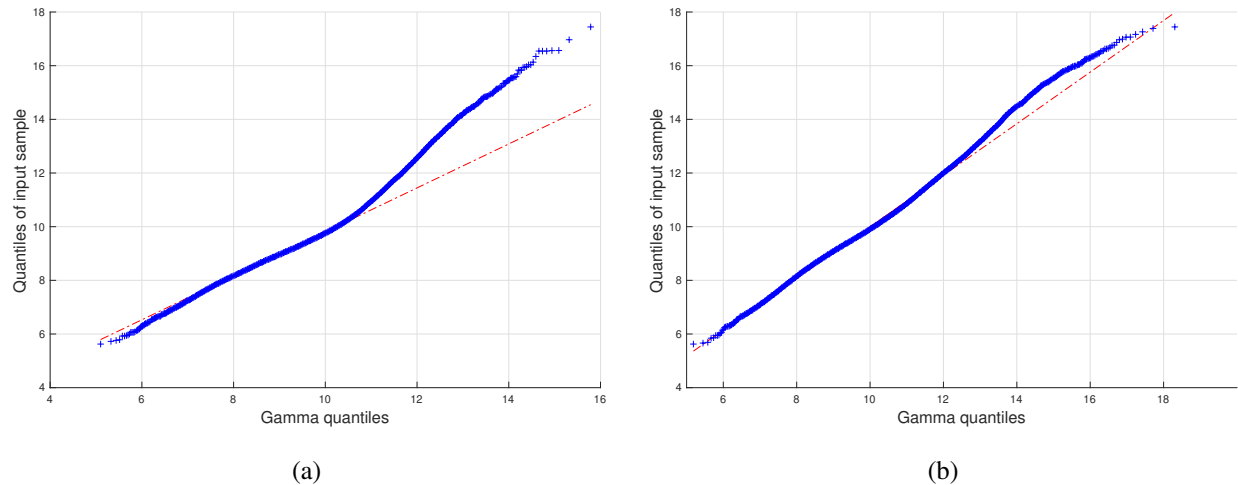


Figure 6: Real-world experiment – Figure (6a) presents the Q-Q plot of the transformed centered temperatures when the average weekly relative humidity is below the constant threshold  $c$  against the fitted Gamma distribution. Figure (6b) shows the corresponding Q-Q plot when the average weekly relative humidity is above the constant threshold  $c$ .

### B. Model Selection

After determining the spatial and temporal fields of interest, we model the measurements of the average weekly relative humidity as noisy samples from a GP with a constant mean function and a Matérn covariance function with  $\nu = 5/2$  defined in (24) with  $r \leftarrow \|x - x'\|$  for  $x, x' \in \mathcal{X}$ . For each week from 03/06/2012 to 29/09/2012, we estimate the signal mean, signal standard deviation, noise standard deviation, and length-scale via *maximum a posteriori* (MAP) estimation (see Chapter 2 of [26] for details) based on the measurements from the 21 weather stations. The prior distributions for logarithms of the signal standard deviation, length-scale, and noise standard deviation are  $\mathcal{N}(-2, 0.1)$ ,  $\mathcal{N}(\log 3.8, 0.1)$ ,  $\mathcal{N}(\log 0.1, 0.01)$ , respectively. The median of the estimated values over 17 weeks are then taken as the final hyperparameters of the GP. The estimated hyperparameters are shown in Table III.

A similar approach is also applied to specify the model for the centered temperatures (CT). For each set of measurements, we model the data after the transformation  $x \mapsto 10 - x$  as noise-free samples from a GP warped by a Gamma random variable. First, the hyperparameters for the Gamma distribution are estimated based on the measurements from the 21 weather stations. Next, the data are transformed by  $z \mapsto \Phi^{-1} \circ F(z)$ , where  $F$  is the CDF of the fitted Gamma distribution. Then, the transformed data are modeled by a GP in which the mean function is constant zero and the covariance function is again the Matérn covariance function with  $\nu = 5/2$  defined in (24). The estimated hyperparameters based on the transformed measurements over all sensors via *maximum marginal likelihood estimation* (see Chapter 5 of [26] for details) are shown in Table IV.

threshold $c$	signal mean	signal std. dev	length-scale	noise std. dev
75.3692	75.0566	5.3068	0.0344	0.1000

Table III: Real-world experiment – Estimated GP hyperparameters

	Gamma( $a, b$ )	GP mean	GP std. dev	GP length-scale
$\mathcal{H}_0$	(53.7457, 0.1771)	0	1	3.7622
$\mathcal{H}_1$	(43.3694, 0.2417)	0	1	4.0654

Table IV: Real-world experiment – Estimated WGP hyperparameters

### C. Experiment Setting

Under the estimated hyperparameters, we construct a binary spatial random field over both a  $50 \times 50$  grid of spatial locations and the 21 weather stations. Then, at each spatial location, a temporal process is generated based on the value of the binary spatial field. We assume all weather stations take point observations, i.e., all are P-sensors. Each sensor collects hourly measurements of the temporal process from 5 : 00 a.m. to 23 : 00 p.m, 7 days a week with  $\sigma_P = 0.1$ . For simplicity, we set  $T = M = 133$ .

Given the point observations, WGPLRT is applied with  $\gamma^P = \exp(-6.5387)$  such that the significance level  $\alpha$  is approximately 0.1, which results in the following transition matrix (see (19))

$$U = \begin{pmatrix} 0.8996 & 0.1004 \\ 0.0774 & 0.9226 \end{pmatrix}. \quad (25)$$

Then, S-BLUE is used to predict the values of the binary spatial field at the  $50 \times 50$  grid of spatial locations where no weather stations are deployed.

### D. Result and Discussion

Figure 7 shows the spatial locations of the 21 weather stations, the true binary spatial random field, and the reconstructed binary spatial field based on the point observations at the 21 weather stations. Figure 8 presents the true latent GP, the reconstructed latent GP, and the map of the Bayes risk given in (22). From Figure (8c), we see that the Bayes risks are small around the weather stations and high over the regions where no weather stations are deployed. The performance of the oracle, S-BLUE, and KNN is presented in Table V. We see that S-BLUE achieves performance comparable to the oracle, showcasing the effectiveness of our proposed algorithm.

Algorithm	MSE	F1 score	FPR	TPR
Oracle	0.3403	0.5962	0.2282	0.5326
S-BLUE	0.3790	0.5544	0.2740	0.5046
KNN	0.4252	0.5391	0.4430	0.5678

Table V: Real-world experiment – Averaged MSE, F1 score, FPR, TPR over 100 realizations.

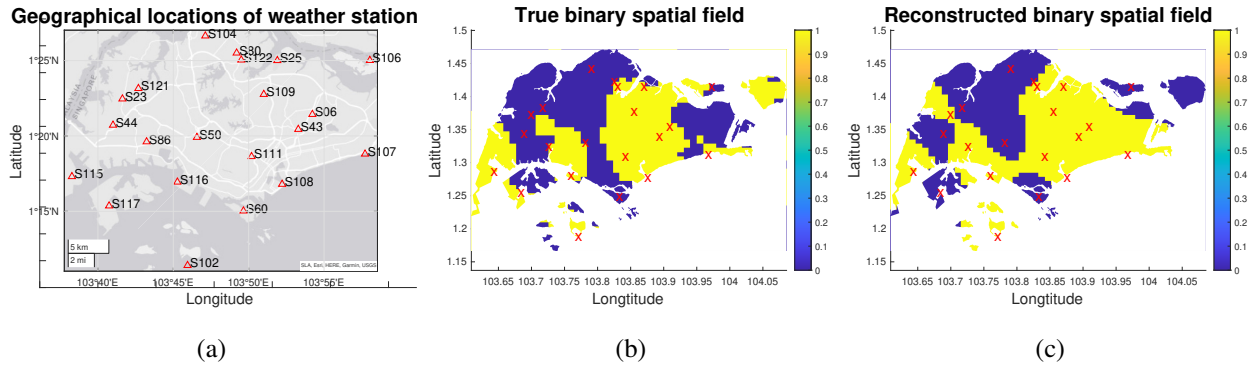


Figure 7: Real-world experiment – Figure (7a) shows the spatial locations of the 21 weather stations over Singapore. Figure (7b) is the true binary spatial field, where the crosses denote the weather stations. Figure (7c) is the reconstructed binary spatial field from our algorithm based on the point observations at the 21 weather stations.

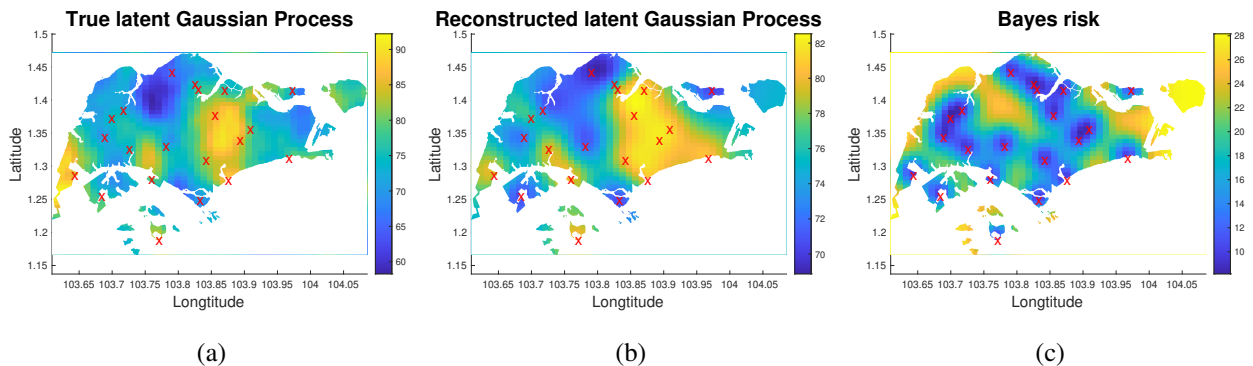


Figure 8: Real-world experiment – Figure (8a) shows the true latent GP. Figure (8b) visualizes the reconstructed latent GP from our algorithm based on the point observations at the 21 weather stations. Figure (8c) shows the map of the Bayes risks defined in (22).

### E. Sensitivity Analysis

In this subsection, we want to analyze the effects of the significance level, number of point observations, and noise variance on the proposed algorithm. To start with, Figure (9a) shows the ROC curve of WGPLRT under the experiment setting specified in Subsection VII-C. To study the impact of the significance level, i.e., FPR, the transition matrix for S-BLUE is determined by points along the ROC curve in Figure (9a) at each significance level. We plot the MSE against the significance level in Figure (9b). Notice that the MSE decreases initially and then increases

because of the trade-off between the TPR and FPR as suggested in Figure (9a).

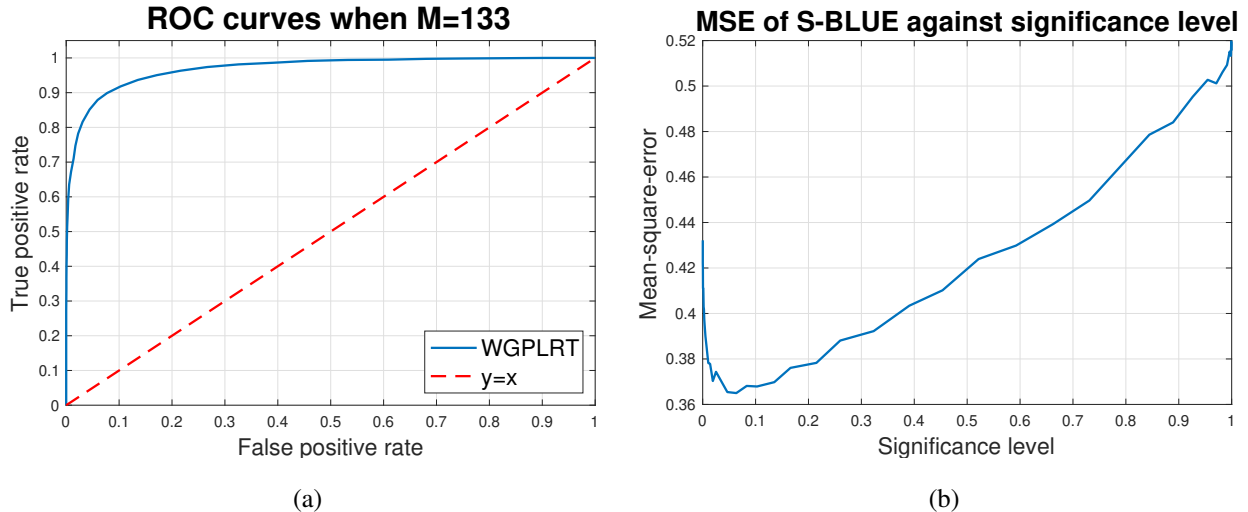


Figure 9: Real-world experiment – Figure (9a) is the ROC curve of WGPLRT under the experiment setting in Subsection VII-C. Figure (9b) shows the MSE of S-BLUE against the significance level.

We proceed to study the effects of the number of point observations and the noise variance. Figure (10a) shows the AUC of WGPLRT against the number of point observations. We observe that though the AUC improves when the number of point observations increases, the slope is close to zero when the number of point observations exceeds approximately 19. Therefore, we take  $M = 19$  when analyzing the effects of the noise variance. Figure (10b) presents the averaged MSE, F1 score, FPR, TPR over 100 realizations against the noise variance. As in the synthetic experiment, the FPR stays relatively constant, the F1 score, TPR increase, and the MSE decreases when the noise variance declines.

## VIII. CONCLUSION

This paper addressed the problem of *binary spatial random field reconstruction* of a hierarchical spatial-temporal system based on sensor observations of the temporal processes. A novel model was proposed to represent a hierarchical spatial-temporal physical phenomenon using WGPS such that the processes may follow arbitrary distributions appeared in real-world applications. A sensor network was deployed over a vast geographical region to monitor the hierarchical spatial-temporal physical phenomenon, where two types of sensors were considered; one collected *point observations* at specific time points while the other collected *integral*

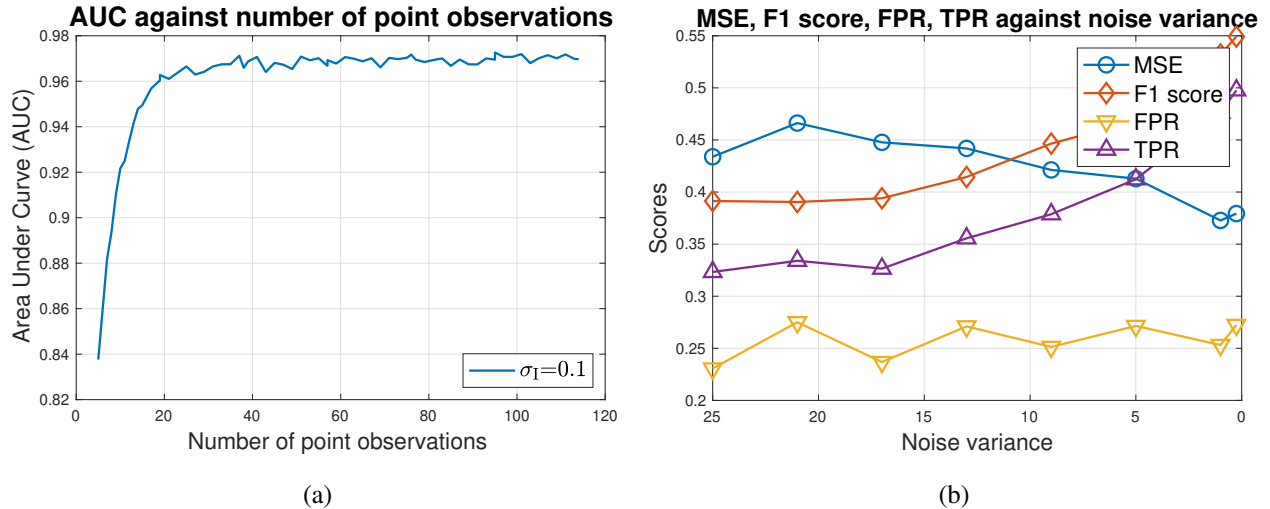


Figure 10: Real-world experiment – Figure (10a) shows the effect of the number of point observations on the AUC of WGPLRT. Figure (10b) presents the averaged MSE, F1 score, FPR, and TPR over 100 realizations against the noise variance of Algorithm 4 when  $M = 19$ .

observations over time intervals. We developed two algorithms: the *Warped Gaussian Process Likelihood Ratio Test (WGPLRT)* and the *Neighborhood-density-based Likelihood Ratio Test (NLRT)* to compress the local sensor observations of the temporal processes to a single-bit. Next, based on the local inferences, we developed the *Spatial Best Linear Unbiased Estimator (S-BLUE)* to solve the problem of binary spatial random field reconstruction. We performed both synthetic experiments and real-world experiments, the latter of which are based on a weather dataset from the National Environment Agency (NEA) of Singapore. The results showed that our proposed algorithm can effectively reconstruct the binary spatial random field.

## IX. ACKNOWLEDGMENTS

The research was conducted under the Undergraduate Research Experience on Campus (URECA) project, supported by the School of Physics and Mathematical Sciences at Nanyang Technological University. AN gratefully acknowledges the financial support by his Nanyang Assistant Professorship Grant (NAP Grant) *Machine Learning based Algorithms in Finance and Insurance*.

## APPENDIX A

## PROOF OF PROPOSITION 5

*Proof of Proposition 5.* Let  $g_* := g(\mathbf{x}_*)$  denote the value of the latent Gaussian Process at a fixed un-monitored position  $\mathbf{x}_* \in \mathcal{X}$ . Note that  $y_* := y(\mathbf{x}_*) \in \{0, 1\}$ , hence Bernoulli( $\pi_*$ ) distributed for some  $\pi_* \in [0, 1]$ . The Bernoulli parameter  $\pi_*$  of the posterior predictive distribution of  $y_*$  conditional on  $(\mathbf{Z}_{1:N^P}^P, \mathbf{Z}_{1:N^I}^I)$  is given by

$$\pi_* = \mathbb{P}(y_* = 1 | \mathbf{Z}_{1:N^P}^P, \mathbf{Z}_{1:N^I}^I) = \int_{\mathbb{R}} \mathbb{P}(y_* = 1 | g_*, \mathbf{Z}_{1:N^P}^P, \mathbf{Z}_{1:N^I}^I) p(g_* | \mathbf{Z}_{1:N^P}^P, \mathbf{Z}_{1:N^I}^I) dg_*. \quad (26)$$

Since  $y_*$  is independent of  $(\mathbf{Z}_{1:N^P}^P, \mathbf{Z}_{1:N^I}^I)$  conditional on  $g_*$  (see Figure 1), we obtain that

$$\mathbb{P}(y_* = 1 | g_*, \mathbf{Z}_{1:N^P}^P, \mathbf{Z}_{1:N^I}^I) = \mathbb{P}(y_* = 1 | g_*) = \mathbb{1}_{\{g_* \geq c\}}, \quad (27)$$

which is a deterministic function of  $g_*$ .

By the Law of Total Probability, the term  $p(g_* | \mathbf{Z}_{1:N^P}^P, \mathbf{Z}_{1:N^I}^I)$  can be written as

$$p(g_* | \mathbf{Z}_{1:N^P}^P, \mathbf{Z}_{1:N^I}^I) = \int_{\mathbb{R}^N} p(g_* | \mathbf{g}, \mathbf{Z}_{1:N^P}^P, \mathbf{Z}_{1:N^I}^I) p(\mathbf{g} | \mathbf{Z}_{1:N^P}^P, \mathbf{Z}_{1:N^I}^I) d\mathbf{g}. \quad (28)$$

Then, by the independence of  $g_*$  and  $(\mathbf{Z}_{1:N^P}^P, \mathbf{Z}_{1:N^I}^I)$  conditional on  $\mathbf{g}$  (see Figure 1), we derive that

$$p(g_* | \mathbf{Z}_{1:N^P}^P, \mathbf{Z}_{1:N^I}^I) = \int_{\mathbb{R}^N} p(g_* | \mathbf{g}) p(\mathbf{g} | \mathbf{Z}_{1:N^P}^P, \mathbf{Z}_{1:N^I}^I) d\mathbf{g}. \quad (29)$$

Moreover, by the Bayes' rule, we have

$$p(\mathbf{g} | \mathbf{Z}_{1:N^P}^P, \mathbf{Z}_{1:N^I}^I) = \frac{p(\mathbf{Z}_{1:N^P}^P, \mathbf{Z}_{1:N^I}^I | \mathbf{g}) p(\mathbf{g})}{\int_{\mathbb{R}^N} p(\mathbf{Z}_{1:N^P}^P, \mathbf{Z}_{1:N^I}^I | \mathbf{g}') p(\mathbf{g}') d\mathbf{g}'}. \quad (30)$$

Due to the conditional independence of  $\{\mathbf{Z}_n^P\}_{n=1:N^P}$ ,  $\{\mathbf{Z}_n^I\}_{n=1:N^I}$  given  $\mathbf{g} = (g(\mathbf{x}_1^P), \dots, g(\mathbf{x}_{N^P}^P), g(\mathbf{x}_1^I), \dots, g(\mathbf{x}_{N^I}^I))$  stated in (TP1), one can factorize  $p(\mathbf{Z}_{1:N^P}^P, \mathbf{Z}_{1:N^I}^I | \mathbf{g})$  as follows

$$p(\mathbf{Z}_{1:N^P}^P, \mathbf{Z}_{1:N^I}^I | \mathbf{g}) = \left( \prod_{n=1}^{N^P} p(\mathbf{Z}_n^P | \mathbf{g}) \right) \left( \prod_{n=1}^{N^I} p(\mathbf{Z}_n^I | \mathbf{g}) \right). \quad (31)$$

Therefore, (26)–(31) imply that  $\mathbb{P}(y_* = 1 | \mathbf{Z}_{1:N^P}^P, \mathbf{Z}_{1:N^I}^I)$  is given by

$$\int_c^\infty \int_{\mathbb{R}^N} p(g_* | \mathbf{g}) \frac{\left( \prod_{n=1}^{N^P} p(\mathbf{Z}_n^P | \mathbf{g}) \right) \left( \prod_{n=1}^{N^I} p(\mathbf{Z}_n^I | \mathbf{g}) \right) p(\mathbf{g})}{\int_{\mathbb{R}^N} \left( \prod_{n=1}^{N^P} p(\mathbf{Z}_n^P | \mathbf{g}') \right) \left( \prod_{n=1}^{N^I} p(\mathbf{Z}_n^I | \mathbf{g}') \right) p(\mathbf{g}') d\mathbf{g}'} d\mathbf{g} dg_*. \quad (32)$$

This proves (7).

Now, let  $y_n^j := y(\mathbf{x}_n^j)$ ,  $g_n^j := g(\mathbf{x}_n^j)$  for  $j \in \{P, I\}$  and observe that

$$\begin{aligned}
& \int_{\mathbb{R}^N} \left( \prod_{n=1}^{N^P} p(\mathbf{Z}_n^P | \mathbf{g}') \right) \left( \prod_{n=1}^{N^I} p(\mathbf{Z}_n^I | \mathbf{g}') \right) p(\mathbf{g}') \, d\mathbf{g}' \\
&= \int_{\mathbb{R}^N} \left( \prod_{n=1}^{N^P} \left( \sum_{l=0,1} p(\mathbf{Z}_n^P | y_n^P = l, \mathbf{g}') p(y_n^P = l | \mathbf{g}') \right) \right) \\
&\quad \times \left( \prod_{n=1}^{N^I} \left( \sum_{l=0,1} p(\mathbf{Z}_n^I | y_n^I = l, \mathbf{g}') p(y_n^I = l | \mathbf{g}') \right) \right) p(\mathbf{g}') \, d\mathbf{g}' \tag{33} \\
&= \int_{\mathbb{R}^N} \left( \prod_{n=1}^{N^P} \left( p(\mathbf{Z}_n^P | y_n^P = 0) \mathbb{1}_{\{g_n^P < c\}} + p(\mathbf{Z}_n^P | y_n^P = 1) \mathbb{1}_{\{g_n^P \geq c\}} \right) \right) \\
&\quad \times \left( \prod_{n=1}^{N^I} \left( p(\mathbf{Z}_n^I | y_n^I = 0) \mathbb{1}_{\{g_n^I < c\}} + p(\mathbf{Z}_n^I | y_n^I = 1) \mathbb{1}_{\{g_n^I \geq c\}} \right) \right) p(\mathbf{g}') \, d\mathbf{g}'.
\end{aligned}$$

Hence, we see that the denominator of the integrand in equation (32) contains a sum of  $2^{N^I+N^P}$  terms and is therefore computationally intractable.  $\square$

## APPENDIX B

### PROOF OF PROPOSITION 6

The following Lemma is needed in the proof of Proposition 6.

**Lemma 15.** *Let  $N \in \mathbb{N}$ , let  $(\mathbf{x}_n)_{n=1:N} \subset \mathcal{X}$ , and let  $\mathbf{z} := (z(\mathbf{x}_1), z(\mathbf{x}_2), \dots, z(\mathbf{x}_N))^\top$  where  $z = W \circ f$  is a WGP defined as in Definition 2 with  $W : \mathbb{R} \rightarrow \text{range}(W) \subseteq \mathbb{R}$  being strictly increasing and continuously differentiable. Let  $W^{-1}$  denote the inverse of  $W$  and let  $\Sigma_{\mathbf{x}_{1:N}}$  denote the covariance matrix of  $f$  evaluated at  $(\mathbf{x}_n)_{n=1:N}$ . Then, the probability density function of  $\mathbf{z}$  is given by*

$$p_{\mathbf{z}}(\mathbf{z}) = \phi_{\mathcal{N}} \left( (W^{-1}(z(\mathbf{x}_1)), \dots, W^{-1}(z(\mathbf{x}_N))) ; \mathbf{0}, \Sigma_{\mathbf{x}_{1:N}} \right) \prod_{i=1}^N \frac{\partial W^{-1}(z(\mathbf{x}_i))}{\partial z(\mathbf{x}_i)}, \tag{34}$$

where  $\phi_{\mathcal{N}}(\cdot; \mathbf{0}, \Sigma_{\mathbf{x}_{1:N}}) : \mathbb{R}^N \rightarrow \mathbb{R}$  denotes the density function of a multivariate normal distribution with mean vector  $\mathbf{0}$  and covariance matrix  $\Sigma_{\mathbf{x}_{1:N}}$ .

Moreover, if  $W := F^{-1} \circ \Phi$ , where  $F$  is strictly increasing and is the CDF of a continuous random variable with continuous density, and  $\Phi$  is the CDF of  $\mathcal{N}(0, 1)$ , then we have

$$p_{\mathbf{z}}(\mathbf{z}) = \phi_{\mathcal{N}} \left( (W^{-1}(z(\mathbf{x}_1)), \dots, W^{-1}(z(\mathbf{x}_N))) ; \mathbf{0}, \Sigma_{\mathbf{x}_{1:N}} \right) \prod_{i=1}^N \frac{F'(z(\mathbf{x}_i))}{\Phi'(\Phi^{-1}(F(z(\mathbf{x}_i))))}. \tag{35}$$

*Proof.* As  $\mathbf{z} = (W(f(\mathbf{x}_1)), \dots, W(f(\mathbf{x}_N)))$  and  $(f(\mathbf{x}_1), \dots, f(\mathbf{x}_N))$  follows a multivariate normal distribution with mean vector  $\mathbf{0}$  and covariance matrix  $\Sigma_{\mathbf{x}_{1:N}}$ , the Change of Variable Theorem (see, e.g., [28, Theorem 10.9]) yields that the joint density of  $\mathbf{z}$  is given by

$$\begin{aligned} p_{\mathbf{z}}(\mathbf{z}) &= \phi_{\mathcal{N}}\left((W^{-1}(z(\mathbf{x}_1)), \dots, W^{-1}(z(\mathbf{x}_N))) ; \mathbf{0}, \Sigma_{\mathbf{x}_{1:N}}\right) \left| \frac{\partial W^{-1}(\mathbf{z})}{\partial \mathbf{z}} \right| \\ &= \phi_{\mathcal{N}}\left((W^{-1}(z(\mathbf{x}_1)), \dots, W^{-1}(z(\mathbf{x}_N))) ; \mathbf{0}, \Sigma_{\mathbf{x}_{1:N}}\right) \det \begin{pmatrix} \frac{\partial W^{-1}(z(\mathbf{x}_1))}{\partial z(\mathbf{x}_1)} & \dots & 0 \\ \vdots & \ddots & \vdots \\ 0 & \dots & \frac{\partial W^{-1}(z(\mathbf{x}_N))}{\partial z(\mathbf{x}_N)} \end{pmatrix}. \end{aligned}$$

Therefore, we obtain that

$$p_{\mathbf{z}}(\mathbf{z}) = \phi_{\mathcal{N}}\left((W^{-1}(z(\mathbf{x}_1)), \dots, W^{-1}(z(\mathbf{x}_N))) ; \mathbf{0}, \Sigma_{\mathbf{x}_{1:N}}\right) \prod_{i=1}^N \frac{\partial W^{-1}(z(\mathbf{x}_i))}{\partial z(\mathbf{x}_i)}, \quad (36)$$

which proves (34).

Moreover, if  $W = F^{-1} \circ \Phi$ , where  $F$  is strictly increasing and is the CDF of a continuous random variable with continuous density, and  $\Phi$  is the CDF of  $\mathcal{N}(0, 1)$ , then  $W$  is also strictly increasing and continuously differentiable. Therefore, since

$$\left. \frac{\partial W^{-1}(y)}{\partial y} \right|_{y=z(\mathbf{x}_i)} = \left. \frac{\partial \Phi^{-1}(F(y))}{\partial y} \right|_{y=z(\mathbf{x}_i)} = \frac{F'(z(\mathbf{x}_i))}{\Phi'(\Phi^{-1}(F(z(\mathbf{x}_i))))}, \quad (37)$$

we can conclude the desired result.  $\square$

*Proof of Proposition 6.* For  $i = 0, 1$ , as  $W_i = F_i^{-1} \circ \Phi$  where  $F_i$  is strictly increasing and is the CDF of a continuous random variable and by Lemma 15, the probability density of the ground-truth values  $\tilde{\mathbf{Z}}_n^{\text{P}}$  of the temporal process  $\tilde{z}$  at  $\mathbf{x}_n^{\text{P}}$  over  $T_{1:M}^{\text{P}}$  with  $G_i := W_i^{-1}$  is given by

$$p(\tilde{\mathbf{Z}}_n^{\text{P}} | \mathcal{H}_i) = (2\pi)^{-\frac{M}{2}} \det(K_i)^{-\frac{1}{2}} \exp\left(-\frac{1}{2} G_i(\tilde{\mathbf{Z}}_n^{\text{P}})^{\text{T}} K_i^{-1} G_i(\tilde{\mathbf{Z}}_n^{\text{P}}) + \sum_{m=1}^M \log \left. \frac{\partial G_i(z)}{\partial z} \right|_{\tilde{z}_{n,m}^{\text{P}}}\right). \quad (38)$$

Since  $\mathbf{Z}_n^{\text{P}} = \tilde{\mathbf{Z}}_n^{\text{P}} + \boldsymbol{\epsilon}_n^{\text{P}}$  and by  $\boldsymbol{\epsilon}_n^{\text{P}} \sim \mathcal{N}(\mathbf{0}, \sigma_{\text{P}}^2 I_M)$ , we have  $\mathbf{Z}_n^{\text{P}} | \tilde{\mathbf{Z}}_n^{\text{P}} \sim \mathcal{N}(\tilde{\mathbf{Z}}_n^{\text{P}}, \sigma_{\text{P}}^2 I_M)$ . Therefore, by the Law of Total Probability, the marginal likelihood of  $\mathbf{Z}_n^{\text{P}}$  is given by

$$\begin{aligned} p(\mathbf{Z}_n^{\text{P}} | \mathcal{H}_i) &= \int_{\mathbb{R}^M} p(\mathbf{Z}_n^{\text{P}} | \tilde{\mathbf{Z}}_n^{\text{P}}; \mathcal{H}_i) p(\tilde{\mathbf{Z}}_n^{\text{P}} | \mathcal{H}_i) d\tilde{\mathbf{Z}}_n^{\text{P}} \\ &= \int_{\mathbb{R}^M} \exp\left(-\frac{1}{2} G_i(\tilde{\mathbf{Z}}_n^{\text{P}})^{\text{T}} K_i^{-1} G_i(\tilde{\mathbf{Z}}_n^{\text{P}}) - \frac{1}{2} \log \det K_i - \frac{M}{2} \log 2\pi \right. \\ &\quad \left. + \sum_{m=1}^M \log \left. \frac{\partial G_i(z)}{\partial z} \right|_{\tilde{z}_{n,m}^{\text{P}}}\right) (2\pi\sigma_{\text{P}}^2)^{-\frac{M}{2}} \exp\left(-\frac{1}{2} \sigma_{\text{P}}^{-2} (\mathbf{Z}_n^{\text{P}} - \tilde{\mathbf{Z}}_n^{\text{P}})^{\text{T}} (\mathbf{Z}_n^{\text{P}} - \tilde{\mathbf{Z}}_n^{\text{P}})\right) d\tilde{\mathbf{Z}}_n^{\text{P}}. \end{aligned} \quad (39)$$

Finally, by applying the Change of Variable Theorem with  $\boldsymbol{\epsilon}_n^{\text{P}} = \mathbf{Z}_n^{\text{P}} - \tilde{\mathbf{Z}}_n^{\text{P}}$ , we conclude that

$$p(\mathbf{Z}_n^{\text{P}}|\mathcal{H}_i) = \int_{\mathbb{R}^M} \exp\left(-\frac{1}{2}G_i(\mathbf{Z}_n^{\text{P}} - \boldsymbol{\epsilon}_n^{\text{P}})^{\text{T}}K_i^{-1}G_i(\mathbf{Z}_n^{\text{P}} - \boldsymbol{\epsilon}_n^{\text{P}}) - \frac{1}{2}\log\det K_i - \frac{M}{2}\log 2\pi\right. \\ \left. + \sum_{m=1}^M \log \frac{\partial G_i(z)}{\partial z} \Big|_{z_{n,m}^{\text{P}} - \epsilon_{n,m}^{\text{P}}}\right) (2\pi\sigma_{\text{P}}^2)^{-\frac{M}{2}} \exp\left(-\frac{1}{2}\sigma_{\text{P}}^{-2}(\boldsymbol{\epsilon}_n^{\text{P}})^{\text{T}}\boldsymbol{\epsilon}_n^{\text{P}}\right) d\boldsymbol{\epsilon}_n^{\text{P}}. \quad (40)$$

□

## APPENDIX C

### PROOF OF PROPOSITION 7

*Proof of Proposition 7.* In the following proof, for the ease of notation, we drop the subscript  $i$ , denote  $\mathbf{Z}_n^{\text{P}}$  as  $\mathbf{z}$ , denote  $\boldsymbol{\epsilon}_n^{\text{P}}$  as  $\boldsymbol{\epsilon}$ , denote  $\hat{p}(\mathbf{Z}_n^{\text{P}}|\mathcal{H}_i)$  as  $\hat{p}(\mathbf{z})$ , and let  $K_M := \mathcal{C}_i(T_{1:M}^{\text{P}}, T_{1:M}^{\text{P}})$  denote the covariance matrix evaluated at  $T_{1:M}^{\text{P}}$ . We have

$$\hat{p}(\mathbf{z}) := \int_{\mathbb{R}^M} \exp\left(\hat{Q}(\mathbf{z} - \boldsymbol{\epsilon}) - \frac{1}{2}\log\det K_M - \frac{M}{2}\log 2\pi\right) (2\pi\sigma_{\text{P}}^2)^{-\frac{M}{2}} \exp\left(-\frac{1}{2}\sigma_{\text{P}}^{-2}\boldsymbol{\epsilon}^{\text{T}}\boldsymbol{\epsilon}\right) d\boldsymbol{\epsilon} \\ = C \int_{\mathbb{R}^M} \exp\left(-\frac{1}{2}(\mathbf{z} - \boldsymbol{\epsilon} - \hat{\mathbf{v}})^{\text{T}}A(\mathbf{z} - \boldsymbol{\epsilon} - \hat{\mathbf{v}}) - \frac{1}{2}\sigma_{\text{P}}^{-2}\boldsymbol{\epsilon}^{\text{T}}\boldsymbol{\epsilon}\right) d\boldsymbol{\epsilon},$$

where the coefficient  $C$  is given by

$$C = \exp\left(-\frac{1}{2}\log\det K_M - \frac{M}{2}\log 2\pi\right) \exp(Q(\hat{\mathbf{v}})) \exp\left(-\frac{M}{2}\log 2\pi - \frac{M}{2}\log\sigma_{\text{P}}^2\right) \\ = \exp\left(-\frac{1}{2}\log\det K_M - M\log 2\pi - M\log\sigma_{\text{P}} + Q(\hat{\mathbf{v}})\right).$$

Therefore, by completing the square and by  $A^{\text{T}} = A$ , we obtain that

$$\hat{p}(\mathbf{z}) = C \int_{\mathbb{R}^M} \exp\left(-\frac{1}{2}(\mathbf{z} - \boldsymbol{\epsilon} - \hat{\mathbf{v}})^{\text{T}}A(\mathbf{z} - \boldsymbol{\epsilon} - \hat{\mathbf{v}}) - \frac{1}{2}\sigma_{\text{P}}^{-2}\boldsymbol{\epsilon}^{\text{T}}\boldsymbol{\epsilon}\right) d\boldsymbol{\epsilon} \\ = C \int_{\mathbb{R}^M} \exp\left(-\frac{1}{2}\left[(\mathbf{z} - \hat{\mathbf{v}})^{\text{T}}A(\mathbf{z} - \hat{\mathbf{v}}) - 2\boldsymbol{\epsilon}^{\text{T}}A(\mathbf{z} - \hat{\mathbf{v}}) + \boldsymbol{\epsilon}^{\text{T}}(A + \sigma_{\text{P}}^{-2}I)\boldsymbol{\epsilon}\right]\right) d\boldsymbol{\epsilon} \\ = C \exp\left(-\frac{1}{2}(\mathbf{z} - \hat{\mathbf{v}})^{\text{T}}A(\mathbf{z} - \hat{\mathbf{v}})\right) \\ \times \int_{\mathbb{R}^M} \exp\left(-\frac{1}{2}\left[\boldsymbol{\epsilon} - (A + \sigma_{\text{P}}^{-2}I)^{-1}A(\mathbf{z} - \hat{\mathbf{v}})\right]^{\text{T}}(A + \sigma_{\text{P}}^{-2}I)\left[\boldsymbol{\epsilon} - (A + \sigma_{\text{P}}^{-2}I)^{-1}A(\mathbf{z} - \hat{\mathbf{v}})\right] \right. \\ \left. + \frac{1}{2}(\mathbf{z} - \hat{\mathbf{v}})^{\text{T}}A(A + \sigma_{\text{P}}^{-2}I)^{-1}A(\mathbf{z} - \hat{\mathbf{v}})\right) d\boldsymbol{\epsilon} \\ = C \exp\left(-\frac{1}{2}(\mathbf{z} - \hat{\mathbf{v}})^{\text{T}}A(\mathbf{z} - \hat{\mathbf{v}}) + \frac{1}{2}(\mathbf{z} - \hat{\mathbf{v}})^{\text{T}}A(A + \sigma_{\text{P}}^{-2}I)^{-1}A(\mathbf{z} - \hat{\mathbf{v}})\right) \\ \times \int_{\mathbb{R}^M} \exp\left(-\frac{1}{2}\left[\boldsymbol{\epsilon} - (A + \sigma_{\text{P}}^{-2}I)^{-1}A(\mathbf{z} - \hat{\mathbf{v}})\right]^{\text{T}}(A + \sigma_{\text{P}}^{-2}I)\left[\boldsymbol{\epsilon} - (A + \sigma_{\text{P}}^{-2}I)^{-1}A(\mathbf{z} - \hat{\mathbf{v}})\right]\right) d\boldsymbol{\epsilon}$$

$$\begin{aligned}
&= C \exp \left( \frac{1}{2} (\mathbf{z} - \widehat{\mathbf{v}})^\top (A(A + \sigma_P^{-2}I)^{-1}A - A) (\mathbf{z} - \widehat{\mathbf{v}}) \right) (2\pi)^{\frac{M}{2}} (\det(A + \sigma_P^{-2}I))^{-\frac{1}{2}} \\
&\quad \times \int_{\mathbb{R}^M} \exp \left( -\frac{1}{2} [\boldsymbol{\epsilon} - (A + \sigma_P^{-2}I)^{-1}A(\mathbf{z} - \widehat{\mathbf{v}})]^\top (A + \sigma_P^{-2}I) [\boldsymbol{\epsilon} - (A + \sigma_P^{-2}I)^{-1}A(\mathbf{z} - \widehat{\mathbf{v}})] \right) \\
&\quad \times (2\pi)^{-\frac{M}{2}} (\det(A + \sigma_P^{-2}I))^{\frac{1}{2}} d\boldsymbol{\epsilon}.
\end{aligned} \tag{41}$$

Moreover, note that the integrand in the last equality is the density function of  $\mathcal{N}(\widehat{\boldsymbol{\mu}}, \widehat{\boldsymbol{\Sigma}})$  with  $\widehat{\boldsymbol{\mu}} := (A + \sigma_P^{-2}I)^{-1}A(\mathbf{z} - \widehat{\mathbf{v}})$  and  $\widehat{\boldsymbol{\Sigma}} := (A + \sigma_P^{-2}I)^{-1}$ , so that

$$\begin{aligned}
&\int_{\mathbb{R}^M} (2\pi)^{-\frac{M}{2}} (\det(A + \sigma_P^{-2}I))^{\frac{1}{2}} \exp \left( -\frac{1}{2} [\boldsymbol{\epsilon} - (A + \sigma_P^{-2}I)^{-1}A(\mathbf{z} - \widehat{\mathbf{v}})]^\top (A + \sigma_P^{-2}I) \right. \\
&\quad \left. \times [\boldsymbol{\epsilon} - (A + \sigma_P^{-2}I)^{-1}A(\mathbf{z} - \widehat{\mathbf{v}})] \right) d\boldsymbol{\epsilon} = 1.
\end{aligned}$$

Combining this with (41) yields that

$$\widehat{p}(\mathbf{z}) = \widehat{C} \exp \left( \frac{1}{2} (\mathbf{z} - \widehat{\mathbf{v}})^\top (A(A + \sigma_P^{-2}I)^{-1}A - A) (\mathbf{z} - \widehat{\mathbf{v}}) \right),$$

where the coefficient  $\widehat{C}$  is defined as follows

$$\begin{aligned}
\widehat{C} &:= \exp \left( -\frac{1}{2} \log \det K_M - M \log 2\pi - M \log \sigma_P + Q(\widehat{\mathbf{v}}) \right) \exp \left( \frac{M}{2} \log 2\pi - \frac{1}{2} \log \det(A + \sigma_P^{-2}I) \right) \\
&= \exp \left( -\frac{1}{2} \log \det K_M - \frac{M}{2} \log 2\pi - M \log \sigma_P + Q(\widehat{\mathbf{v}}) - \frac{1}{2} \log \det(A + \sigma_P^{-2}I) \right).
\end{aligned}$$

Finally, using the Woodbury's matrix identity (with  $Z \leftarrow A^{-1}$ ,  $U \leftarrow I$ ,  $V \leftarrow I$ , and  $W \leftarrow \sigma_P^2 I$  in the notation of Appendix A.3 in [26]), we therefore see that

$$\widehat{p}(\mathbf{z}) = \widehat{C} \exp \left( -\frac{1}{2} (\mathbf{z} - \widehat{\mathbf{v}})^\top (A^{-1} + \sigma_P^2 I)^{-1} (\mathbf{z} - \widehat{\mathbf{v}}) \right).$$

□

## APPENDIX D

### PROOF OF THEOREM 12

In order to derive the analytic expression for the S-BLUE, the following Lemma is needed. Let  $g_* := g(\mathbf{x}_*)$  denote the value of the latent GP at a fixed un-monitored position  $\mathbf{x}_* \in \mathcal{X}$ .

**Lemma 16.** *The conditional predictive distribution of  $g_*$  given  $\mathbf{g}$  is  $\mathcal{N}(\mu_{g_*|\mathbf{g}}, \sigma_{g_*|\mathbf{g}}^2)$  with*

$$\mu_{g_*|\mathbf{g}} := \mu(\mathbf{x}_*) + \mathcal{C}(\mathbf{x}_*, X_{1:N}) \mathcal{C}(X_{1:N}, X_{1:N})^{-1} (\mathbf{g} - \mu(X_{1:N})),$$

$$\sigma_{g_*|g}^2 := \mathcal{C}(\mathbf{x}_*, \mathbf{x}_*) - \mathcal{C}(\mathbf{x}_*, X_{1:N})\mathcal{C}(X_{1:N}, X_{1:N})^{-1}\mathcal{C}(X_{1:N}, \mathbf{x}_*).$$

*Proof.* Since  $g$  is a GP, the joint distribution of  $\mathbf{g}$  and  $g_*$  follows a multivariate normal distribution given by

$$\begin{bmatrix} \mathbf{g} \\ g_* \end{bmatrix} \sim \mathcal{N} \left( \begin{bmatrix} \mu(X_{1:N}) \\ \mu(\mathbf{x}_*) \end{bmatrix}, \begin{bmatrix} \mathcal{C}(X_{1:N}, X_{1:N}) & \mathcal{C}(X_{1:N}, \mathbf{x}_*) \\ \mathcal{C}(\mathbf{x}_*, X_{1:N}) & \mathcal{C}(\mathbf{x}_*, \mathbf{x}_*) \end{bmatrix} \right). \quad (42)$$

Hence, the result follows from the property of the multivariate normal distribution, see, e.g., Appendix A.2 in [26].  $\square$

*Proof of Theorem 12.* Under the quadratic loss function, the Bayes risk  $\mathcal{R}[h]$  for any  $h \in \mathcal{H}$  is given by

$$\begin{aligned} \mathcal{R}[h] &= \mathbb{E} \left[ (\mathbf{w}^\top \widehat{\mathbf{Y}}_{1:N} + b - g_*)^2 \right] \\ &= \mathbf{w}^\top \mathbb{E} \left[ \widehat{\mathbf{Y}}_{1:N} \widehat{\mathbf{Y}}_{1:N}^\top \right] \mathbf{w} + b^2 - 2b\mathbb{E}[g_*] + \mathbb{E}[g_*^2] + 2\mathbf{w}^\top \mathbb{E}[\widehat{\mathbf{Y}}_{1:N}]b - 2\mathbf{w}^\top \mathbb{E}[\widehat{\mathbf{Y}}_{1:N}g_*]. \end{aligned} \quad (43)$$

Let  $\mu_* := \mathbb{E}[g_*] = \mu(\mathbf{x}_*)$ . Differentiating  $\mathcal{R}[h]$  with respect to  $\mathbf{w}$  and  $b$  yields that

$$\begin{aligned} \frac{\partial \mathcal{R}}{\partial \mathbf{w}} &= 2\mathbb{E}[\widehat{\mathbf{Y}}_{1:N} \widehat{\mathbf{Y}}_{1:N}^\top] \mathbf{w} + 2b\mathbb{E}[\widehat{\mathbf{Y}}_{1:N}] - 2\mathbb{E}[\widehat{\mathbf{Y}}_{1:N}g_*], \\ \frac{\partial \mathcal{R}}{\partial b} &= 2b - 2\mu_* + 2\mathbf{w}^\top \mathbb{E}[\widehat{\mathbf{Y}}_{1:N}]. \end{aligned} \quad (44)$$

Setting the partial derivatives to zero, we obtain that

$$\begin{aligned} b &= \mu_* - \mathbf{w}^\top \mathbb{E}[\widehat{\mathbf{Y}}_{1:N}], \\ \mathbf{w} &= \left( \mathbb{E}[\widehat{\mathbf{Y}}_{1:N} \widehat{\mathbf{Y}}_{1:N}^\top] - \mathbb{E}[\widehat{\mathbf{Y}}_{1:N}]\mathbb{E}[\widehat{\mathbf{Y}}_{1:N}]^\top \right)^{-1} \left( \mathbb{E}[\widehat{\mathbf{Y}}_{1:N}g_*] - \mu_*\mathbb{E}[\widehat{\mathbf{Y}}_{1:N}] \right) \\ &= \text{Cov}[\widehat{\mathbf{Y}}_{1:N}]^{-1} \text{Cov}[\widehat{\mathbf{Y}}_{1:N}, g_*]. \end{aligned} \quad (45)$$

Therefore, the S-BLUE is given by

$$\widehat{h}_{\text{S-BLUE}}(\widehat{\mathbf{Y}}_{1:N}) = \mu_* + \text{Cov}[g_*, \widehat{\mathbf{Y}}_{1:N}] \text{Cov}[\widehat{\mathbf{Y}}_{1:N}]^{-1} (\widehat{\mathbf{Y}}_{1:N} - \mathbb{E}[\widehat{\mathbf{Y}}_{1:N}]). \quad (46)$$

The mean and covariance terms involved in the S-BLUE are presented below. For the ease of notation, let  $g_i := g(\mathbf{x}_i)$ ,  $y_i := y(\mathbf{x}_i)$ ,  $\mu_i := \mu(\mathbf{x}_i)$ , and  $\sigma_i^2 := \mathcal{C}(\mathbf{x}_i, \mathbf{x}_i)$  for  $i = 1 \dots, N$ . Therefore, for  $i = 1, \dots, N$ , as  $g_i \sim \mathcal{N}(\mu_i, \sigma_i^2)$ ,

$$\begin{aligned} \mathbb{E}[\widehat{y}_i] &= \mathbb{E}[\widehat{y}_i | y_i = 1] \mathbb{P}[y_i = 1] + \mathbb{E}[\widehat{y}_i | y_i = 0] \mathbb{P}[y_i = 0] \\ &= p_{11}^i \mathbb{P}[g_i \geq c] + p_{01}^i \mathbb{P}[g_i < c] \\ &= p_{11}^i \Phi \left( -\frac{c - \mu_i}{\sigma_i} \right) + p_{01}^i \Phi \left( \frac{c - \mu_i}{\sigma_i} \right). \end{aligned} \quad (47)$$

Similarly, for  $i, j = 1, \dots, N$ , due to the conditional independence of  $\{\mathbf{Z}_n^P\}_{n=1:N^P}$ ,  $\{\mathbf{Z}_n^I\}_{n=1:N^I}$  given  $(g(\mathbf{x}_1^P), \dots, g(\mathbf{x}_{N^P}^P), g(\mathbf{x}_1^I), \dots, g(\mathbf{x}_{N^I}^I))$  stated in (TP1), we have

$$\begin{aligned}\mathbb{E}[\widehat{y}_i \widehat{y}_j] &= \mathbb{E}[\mathbb{E}[\widehat{y}_i \widehat{y}_j | g_i, g_j]] \\ &= \mathbb{E}[\mathbb{E}[\widehat{y}_i | g_i, g_j] \mathbb{E}[\widehat{y}_j | g_i, g_j]],\end{aligned}\tag{48}$$

where  $(g_i, g_j)^\top \sim \mathcal{N}\left(\begin{pmatrix} \mu_i \\ \mu_j \end{pmatrix}, \begin{pmatrix} \sigma_i^2 & c(\mathbf{x}_i, \mathbf{x}_j) \\ c(\mathbf{x}_i, \mathbf{x}_j) & \sigma_j^2 \end{pmatrix}\right)$ . Moreover, by Remark 11, we have, for  $i = 1, \dots, N$ ,  $\mathbb{E}[\widehat{y}_i | g_i] = p_{11}^i \mathbb{1}_{\{g_i \geq c\}} + p_{01}^i \mathbb{1}_{\{g_i < c\}}$ . Therefore, we see that  $\mathbb{E}[\widehat{y}_i | g_i]$  is  $\sigma(g_i)$ -measurable, where  $\sigma(g_i)$  denotes the  $\sigma$ -algebra generated by  $g_i$ . Then (48) becomes

$$\begin{aligned}\mathbb{E}[\widehat{y}_i \widehat{y}_j] &= \mathbb{E}[\mathbb{E}[\widehat{y}_i | g_i] \mathbb{E}[\widehat{y}_j | g_j]] \\ &= \mathbb{E}[(p_{11}^i \mathbb{1}_{\{g_i \geq c\}} + p_{01}^i \mathbb{1}_{\{g_i < c\}})(p_{11}^j \mathbb{1}_{\{g_j \geq c\}} + p_{01}^j \mathbb{1}_{\{g_j < c\}})] \\ &= p_{01}^i p_{01}^j \mathbb{E}[\mathbb{1}_{\{g_i < c, g_j < c\}}] + p_{01}^i p_{11}^j \mathbb{E}[\mathbb{1}_{\{g_i < c, g_j \geq c\}}] \\ &\quad + p_{11}^i p_{01}^j \mathbb{E}[\mathbb{1}_{\{g_i \geq c, g_j < c\}}] + p_{11}^i p_{11}^j \mathbb{E}[\mathbb{1}_{\{g_i \geq c, g_j \geq c\}}] \\ &= p_{01}^i p_{01}^j \mathbb{P}(g_i < c, g_j < c) + p_{01}^i p_{11}^j \mathbb{P}(g_i < c, g_j \geq c) \\ &\quad + p_{11}^i p_{01}^j \mathbb{P}(g_i \geq c, g_j < c) + p_{11}^i p_{11}^j \mathbb{P}(g_i \geq c, g_j \geq c).\end{aligned}\tag{49}$$

Then, the covariance  $\text{Cov}[\widehat{y}_i, \widehat{y}_j]$  is given by

$$\begin{aligned}\text{Cov}[\widehat{y}_i, \widehat{y}_j] &= \mathbb{E}[\widehat{y}_i \widehat{y}_j] - \mathbb{E}[\widehat{y}_i] \mathbb{E}[\widehat{y}_j] \\ &= p_{01}^i p_{01}^j \mathbb{P}(g_i < c, g_j < c) + p_{01}^i p_{11}^j \mathbb{P}(g_i < c, g_j \geq c) \\ &\quad + p_{11}^i p_{01}^j \mathbb{P}(g_i \geq c, g_j < c) + p_{11}^i p_{11}^j \mathbb{P}(g_i \geq c, g_j \geq c) \\ &\quad - \left[ p_{11}^i \Phi\left(-\frac{c - \mu_i}{\sigma_i}\right) + p_{01}^i \Phi\left(\frac{c - \mu_i}{\sigma_i}\right) \right] \left[ p_{11}^j \Phi\left(-\frac{c - \mu_j}{\sigma_j}\right) + p_{01}^j \Phi\left(\frac{c - \mu_j}{\sigma_j}\right) \right].\end{aligned}\tag{50}$$

Finally, for  $i = 1, \dots, N$ , by the conditional independence of  $g_*$  and  $\widehat{y}_i$  given  $g_i$  (see Figure 1), we obtain that

$$\begin{aligned}\mathbb{E}[\widehat{y}_i g_*] &= \mathbb{E}[\mathbb{E}[g_* \widehat{y}_i | g_i]] \\ &= \mathbb{E}[\mathbb{E}[g_* | \widehat{y}_i = 1, g_i] \mathbb{P}(\widehat{y}_i = 1 | g_i)] \\ &= \mathbb{E}[\mathbb{E}[g_* | g_i] \mathbb{P}(\widehat{y}_i = 1 | g_i)] \\ &= \mathbb{E}\left[\mathbb{E}[g_* | g_i] \left( \mathbb{P}(\widehat{y}_i = 1 | y_i = 1, g_i) \mathbb{P}(y_i = 1 | g_i) + \mathbb{P}(\widehat{y}_i = 1 | y_i = 0, g_i) \mathbb{P}(y_i = 0 | g_i) \right)\right] \\ &= \mathbb{E}\left[\mathbb{E}[g_* | g_i] \left( p_{11}^i \mathbb{1}_{\{g_i \geq c\}} + p_{01}^i \mathbb{1}_{\{g_i < c\}} \right)\right].\end{aligned}\tag{51}$$

By Lemma 16, we have  $\mathbb{E}[g_*|g_i] = \mu_* + \mathcal{C}(\mathbf{x}_*, \mathbf{x}_i)(g_i - \mu_i)/\sigma_i^2$ , then (51) becomes

$$\begin{aligned}
\mathbb{E}[\widehat{y}_i g_*] &= \mu_* \left( p_{11}^i \mathbb{E}[\mathbb{1}_{\{g_i \geq c\}}] + p_{01}^i \mathbb{E}[\mathbb{1}_{\{g_i < c\}}] \right) \\
&\quad + \mathcal{C}(\mathbf{x}_*, \mathbf{x}_i) \left( p_{11}^i \mathbb{E} \left[ \frac{(g_i - \mu_i)}{\sigma_i^2} \mathbb{1}_{\{g_i \geq c\}} \right] + p_{01}^i \mathbb{E} \left[ \frac{(g_i - \mu_i)}{\sigma_i^2} \mathbb{1}_{\{g_i < c\}} \right] \right) \\
&= \mu_* \left( p_{11}^i \Phi \left( -\frac{c - \mu_i}{\sigma_i} \right) + p_{01}^i \Phi \left( \frac{c - \mu_i}{\sigma_i} \right) \right) \\
&\quad + \mathcal{C}(\mathbf{x}_*, \mathbf{x}_i) \left( p_{11}^i \int_{\{g_i \geq c\}} \frac{g_i - \mu_i}{\sqrt{2\pi}\sigma_i^3} \exp \left( -\frac{(g_i - \mu_i)^2}{2\sigma_i^2} \right) dg_i \right. \\
&\quad \left. + p_{01}^i \int_{\{g_i < c\}} \frac{g_i - \mu_i}{\sqrt{2\pi}\sigma_i^3} \exp \left( -\frac{(g_i - \mu_i)^2}{2\sigma_i^2} \right) dg_i \right). \tag{52}
\end{aligned}$$

Let  $u = \frac{g_i - \mu_i}{\sigma_i}$ , we obtain that

$$\int_{\{g_i \geq c\}} \frac{g_i - \mu_i}{\sqrt{2\pi}\sigma_i^3} \exp \left( -\frac{(g_i - \mu_i)^2}{2\sigma_i^2} \right) dg_i = \int_{\frac{c - \mu_i}{\sigma_i}}^{\infty} \frac{u}{\sqrt{2\pi}\sigma_i} \exp(-u^2/2) du, \tag{53}$$

and

$$\int_{\{g_i < c\}} \frac{g_i - \mu_i}{\sqrt{2\pi}\sigma_i^3} \exp \left( -\frac{(g_i - \mu_i)^2}{2\sigma_i^2} \right) dg_i = \int_{-\infty}^{\frac{c - \mu_i}{\sigma_i}} \frac{u}{\sqrt{2\pi}\sigma_i} \exp(-u^2/2) du. \tag{54}$$

Subsequently, since  $\mathbb{R} \ni u \mapsto u \exp(-u^2/2) \in \mathbb{R}$  is an odd function, we have

$$\int_{\frac{c - \mu_i}{\sigma_i}}^{\infty} \frac{u}{\sqrt{2\pi}\sigma_i} \exp(-u^2/2) du + \int_{-\infty}^{\frac{c - \mu_i}{\sigma_i}} \frac{u}{\sqrt{2\pi}\sigma_i} \exp(-u^2/2) du = 0. \tag{55}$$

If  $c \geq \mu_i$ , then using the substitution  $u \mapsto v := u^2/2$  gives

$$\int_{\frac{c - \mu_i}{\sigma_i}}^{\infty} \frac{u}{\sqrt{2\pi}\sigma_i} \exp(-u^2/2) du = \int_{\frac{(c - \mu_i)^2}{2\sigma_i^2}}^{\infty} \frac{1}{\sqrt{2\pi}\sigma_i} \exp(-v) dv = \frac{1}{\sqrt{2\pi}\sigma_i} \exp \left( -\frac{(c - \mu_i)^2}{2\sigma_i^2} \right). \tag{56}$$

If  $c < \mu_i$ , then using (55) and the substitution  $u \mapsto v := (-u)^2/2$  yields that

$$\begin{aligned}
\int_{\frac{c - \mu_i}{\sigma_i}}^{\infty} \frac{u}{\sqrt{2\pi}\sigma_i} \exp(-u^2/2) du &= - \int_{-\infty}^{\frac{c - \mu_i}{\sigma_i}} \frac{u}{\sqrt{2\pi}\sigma_i} \exp(-u^2/2) du \\
&= \int_{\frac{(c - \mu_i)^2}{2\sigma_i^2}}^{\infty} \frac{1}{\sqrt{2\pi}\sigma_i} \exp(-v) dv \\
&= \frac{1}{\sqrt{2\pi}\sigma_i} \exp \left( -\frac{(c - \mu_i)^2}{2\sigma_i^2} \right). \tag{57}
\end{aligned}$$

Therefore,  $\mu_* := \mathbb{E}[g_*]$ , (47), and (52)–(57) imply that

$$\begin{aligned}
\text{Cov}[g_*, \widehat{y}_i] &= \mathbb{E}[\widehat{y}_i g_*] - \mathbb{E}[\widehat{y}_i] \mathbb{E}[g_*] \\
&= \mu_* \left( p_{11}^i \Phi \left( -\frac{c - \mu_i}{\sigma_i} \right) + p_{01}^i \Phi \left( \frac{c - \mu_i}{\sigma_i} \right) \right) \\
&\quad + \frac{1}{\sqrt{2\pi}\sigma_i} \mathcal{C}(\mathbf{x}_*, \mathbf{x}_i) \left( p_{11}^i \exp \left( -\frac{(c - \mu_i)^2}{2\sigma_i^2} \right) - p_{01}^i \exp \left( -\frac{(c - \mu_i)^2}{2\sigma_i^2} \right) \right) \\
&\quad - \mu_* \left( p_{11}^i \Phi \left( -\frac{c - \mu_i}{\sigma_i} \right) + p_{01}^i \Phi \left( \frac{c - \mu_i}{\sigma_i} \right) \right) \\
&= \frac{1}{\sqrt{2\pi}\sigma_i} (p_{11}^i - p_{01}^i) \mathcal{C}(\mathbf{x}_*, \mathbf{x}_i) \exp \left( -\frac{(c - \mu_i)^2}{2\sigma_i^2} \right).
\end{aligned} \tag{58}$$

□

## APPENDIX E

### PROOF OF COROLLARY 14

*Proof.* Substitute (20) into (17), then the Bayes risk  $\mathcal{R}[\widehat{h}_{\text{S-BLUE}}(\widehat{\mathbf{Y}}_{1:N})]$  associated with  $\widehat{h}_{\text{S-BLUE}}(\widehat{\mathbf{Y}}_{1:N})$  is given by

$$\begin{aligned}
&\mathbb{E}[(\widehat{h}_{\text{S-BLUE}}(\widehat{\mathbf{Y}}_{1:N}) - g_*)^2] \\
&= \mathbb{E} \left[ \left( \mu_* + \text{Cov}[g_*, \widehat{\mathbf{Y}}_{1:N}] \text{Cov}[\widehat{\mathbf{Y}}_{1:N}]^{-1} (\widehat{\mathbf{Y}}_{1:N} - \mathbb{E}[\widehat{\mathbf{Y}}_{1:N}]) - g_* \right)^2 \right] \\
&= \mathbb{E} \left[ (g_* - \mu_*)^2 - 2(g_* - \mu_*) \text{Cov}[g_*, \widehat{\mathbf{Y}}_{1:N}] \text{Cov}[\widehat{\mathbf{Y}}_{1:N}]^{-1} (\widehat{\mathbf{Y}}_{1:N} - \mathbb{E}[\widehat{\mathbf{Y}}_{1:N}]) \right. \\
&\quad \left. + \text{Cov}[g_*, \widehat{\mathbf{Y}}_{1:N}] \text{Cov}[\widehat{\mathbf{Y}}_{1:N}]^{-1} (\widehat{\mathbf{Y}}_{1:N} - \mathbb{E}[\widehat{\mathbf{Y}}_{1:N}]) (\widehat{\mathbf{Y}}_{1:N} - \mathbb{E}[\widehat{\mathbf{Y}}_{1:N}])^\top \text{Cov}[\widehat{\mathbf{Y}}_{1:N}]^{-1} \text{Cov}[g_*, \widehat{\mathbf{Y}}_{1:N}]^\top \right].
\end{aligned} \tag{59}$$

Since  $\text{Cov}[g_*, \widehat{\mathbf{Y}}_{1:N}]$ ,  $\text{Cov}[\widehat{\mathbf{Y}}_{1:N}]$  are constant matrices once  $\mathbf{x}_*$  and  $\mathbf{X}_{1:N}$  are known (see (21) in Theorem 12), we have

$$\begin{aligned}
&\mathbb{E}[(\widehat{h}_{\text{S-BLUE}}(\widehat{\mathbf{Y}}_{1:N}) - g_*)^2] \\
&= \text{Cov}[g_*] - 2\text{Cov}[g_*, \widehat{\mathbf{Y}}_{1:N}] \text{Cov}[\widehat{\mathbf{Y}}_{1:N}]^{-1} \mathbb{E} \left[ (\widehat{\mathbf{Y}}_{1:N} - \mathbb{E}[\widehat{\mathbf{Y}}_{1:N}]) (g_* - \mu_*) \right] \\
&\quad + \text{Cov}[g_*, \widehat{\mathbf{Y}}_{1:N}] \text{Cov}[\widehat{\mathbf{Y}}_{1:N}]^{-1} \mathbb{E} \left[ (\widehat{\mathbf{Y}}_{1:N} - \mathbb{E}[\widehat{\mathbf{Y}}_{1:N}]) (\widehat{\mathbf{Y}}_{1:N} - \mathbb{E}[\widehat{\mathbf{Y}}_{1:N}])^\top \right] \text{Cov}[\widehat{\mathbf{Y}}_{1:N}]^{-1} \text{Cov}[g_*, \widehat{\mathbf{Y}}_{1:N}]^\top \\
&= \text{Cov}[g_*] - 2\text{Cov}[g_*, \widehat{\mathbf{Y}}_{1:N}] \text{Cov}[\widehat{\mathbf{Y}}_{1:N}]^{-1} \text{Cov}[g_*, \widehat{\mathbf{Y}}_{1:N}]^\top \\
&\quad + \text{Cov}[g_*, \widehat{\mathbf{Y}}_{1:N}] \text{Cov}[\widehat{\mathbf{Y}}_{1:N}]^{-1} \text{Cov}[\widehat{\mathbf{Y}}_{1:N}] \text{Cov}[\widehat{\mathbf{Y}}_{1:N}]^{-1} \text{Cov}[g_*, \widehat{\mathbf{Y}}_{1:N}]^\top \\
&= \text{Cov}[g_*] - \text{Cov}[g_*, \widehat{\mathbf{Y}}_{1:N}] \text{Cov}[\widehat{\mathbf{Y}}_{1:N}]^{-1} \text{Cov}[g_*, \widehat{\mathbf{Y}}_{1:N}]^\top.
\end{aligned} \tag{60}$$

□

## REFERENCES

- [1] Akyildiz, I., Su, W., Sankarasubramaniam, Y., and Cayirci, E. (2002). Wireless sensor networks: a survey. *Computer Networks*, 38(4):393–422.
- [2] Beyer, K., Goldstein, J., Ramakrishnan, R., and Shaft, U. (1999). When is “nearest neighbor” meaningful? In *Database Theory — ICDT’99*. Springer.
- [3] Box, G. E., Jenkins, G. M., Reinsel, G. C., and Ljung, G. M. (2015). *Time series analysis: forecasting and control, 5th Edition*. John Wiley & Sons.
- [4] Chintalapudi, K., Fu, T., Paek, J., Kothari, N., Rangwala, S., Caffrey, J., Govindan, R., Johnson, E., and Masri, S. (2006). Monitoring civil structures with a wireless sensor network. *IEEE Internet Computing*, 10(2):26–34.
- [5] Chiu, W.-Y. and Chen, B.-S. (2011). Multisource prediction under nonlinear dynamics in WSNs using a robust fuzzy approach. *IEEE Transactions on Circuits and Systems I: Regular Papers*, 58(1):137–149.
- [6] Cohen, K. and Leshem, A. (2011). Energy-efficient detection in wireless sensor networks using likelihood ratio and channel state information. *IEEE Journal on Selected Areas in Communications*, 29:1671–1683.
- [7] Embrechts, P., Resnick, S. I., and Samorodnitsky, G. (1999). Extreme value theory as a risk management tool. *North American Actuarial Journal*, 3(2):30–41.
- [8] Falkner, P., Peacock, A., and Schulz, R. (2007). Instrumentation for planetary exploration missions. *Treatise on Geophysics*, 10:595–641.
- [9] Fazel, F., Fazel, M., and Stojanovic, M. (2012). Random access sensor networks: Field reconstruction from incomplete data. In *2012 Information Theory and Applications Workshop*, pages 300–305.
- [10] French, J. P. and Sain, S. R. (2013). Spatio-temporal exceedance locations and confidence regions. *The Annals of Applied Statistics*, 7(3):1421–1449.
- [11] Gelfand, A. E. and Shirota, S. (2019). Preferential sampling for presence/absence data and for fusion of presence/absence data with presence-only data. *Ecological Monographs*, 89(3):1–17.
- [12] Hart, J. K. and Martinez, K. (2006). Environmental sensor networks: A revolution in the earth system science? *Earth-Science Reviews*, 78(3):177–191.
- [13] Heagerty, P. J. and Lele, S. R. (1998). A composite likelihood approach to binary spatial

- data. *Journal of the American Statistical Association*, 93(443):1099–1111.
- [14] Kottas, A., Wang, Z., and Rodríguez, A. (2012). Spatial modeling for risk assessment of extreme values from environmental time series: a Bayesian nonparametric approach. *Environmetrics*, 23:649–662.
- [15] Lázaro-Gredilla, M. (2012). Bayesian warped Gaussian processes. In *Proceedings of the 25th International Conference on Neural Information Processing Systems - Volume 1*, pages 1619–1627. Curran Associates Inc.
- [16] Lee, S.-H. and Blake, R. (1999). Detection of temporal structure depends on spatial structure. *Vision Research*, 39(18):3033–3048.
- [17] Luo, J. and Cao, Z. (2015). Distributed detection in wireless sensor networks under Byzantine attacks. *International Journal of Distributed Sensor Networks*, 2015:1–18.
- [18] Luo, Z.-Q. (2005). Universal decentralized estimation in a bandwidth constrained sensor network. *IEEE Transactions on Information Theory*, 51(6):2210–2219.
- [19] Maşazade, E., Niu, R., Varshney, P. K., and Keskinöz, M. (2010). Energy aware iterative source localization for wireless sensor networks. *IEEE Transactions on Signal Processing*, 58(9):4824–4835.
- [20] Msechu, E. J. and Giannakis, G. B. (2012). Sensor-centric data reduction for estimation with WSNs via censoring and quantization. *IEEE Transactions on Signal Processing*, 60:400–414.
- [21] Nevat, I., Peters, G. W., and Collings, I. B. (2014). Distributed detection in sensor networks over fading channels with multiple antennas at the fusion centre. *IEEE Transactions on Signal Processing*, 62(3):671–683.
- [22] Nevat, I., Peters, G. W., Septier, F., and Matsui, T. (2015). Estimation of spatially correlated random fields in heterogeneous wireless sensor networks. *IEEE Transactions on Signal Processing*, 63(10):2597–2609.
- [23] Neyman, J. and Pearson, E. S. (1933). On the problem of the most efficient tests of statistical hypotheses. *Philosophical Transactions of the Royal Society of London. Series A, Containing Papers of a Mathematical or Physical Character*, 231:289–337.
- [24] Peters, G. W., Nevat, I., Nagarajan, S. G., and Matsui, T. (2021). Spatial warped Gaussian processes: Estimation and efficient field reconstruction. *Entropy*, 23(10).
- [25] Rajasegarar, S., Zhang, P., Zhou, Y., Karunasekera, S., Leckie, C., and Palaniswami, M. (2014). High resolution spatio-temporal monitoring of air pollutants using wireless sensor networks. In *2014 IEEE Ninth International Conference on Intelligent Sensors, Sensor*

- Networks and Information Processing (ISSNIP)*, pages 1–6.
- [26] Rasmussen, C. E. and Williams, C. K. I. (2005). *Gaussian Processes for Machine Learning (Adaptive Computation and Machine Learning)*. The MIT Press.
- [27] Rios, G. and Tobar, F. (2019). Compositionally-warped Gaussian processes. *Neural Networks*, 118:235–246.
- [28] Rudin, W. (1976). *Principles of mathematical analysis*, volume 3. McGraw-hill.
- [29] Snelson, E., Ghahramani, Z., and Rasmussen, C. (2003). Warped Gaussian processes. In *Advances in Neural Information Processing Systems*, volume 16. MIT Press.
- [30] Sohraby, K., Minoli, D., and Znati, T. (2006). Wireless sensor networks: Technology, protocols, and applications. *Wireless Sensor Networks: Technology, Protocols, and Applications*, pages 1–307.
- [31] Toni, T., Welch, D., Strelkowa, N., Ipsen, A., and Stumpf, M. P. (2008). Approximate Bayesian computation scheme for parameter inference and model selection in dynamical systems. *Journal of The Royal Society Interface*, 6(31):187–202.
- [32] Vinokur, I. and Tolpin, D. (2021). Warped input Gaussian processes for time series forecasting. In *International Symposium on Cyber Security Cryptography and Machine Learning*, pages 205–220. Springer.
- [33] Xia, Y. and Kamel, M. S. (2008). Cooperative learning algorithms for data fusion using novel  $l_1$  estimation. *IEEE Transactions on Signal Processing*, 56(3):1083–1095.
- [34] Xiang, Q., Neufeld, A., Peters, G. W., Nevat, I., and Datta, A. (2021). A bonus-malus framework for cyber risk insurance and optimal cybersecurity provisioning. *Preprint, arXiv:0706.1234 [math.FA]*.
- [35] Xiang, Q., Nevat, I., and Peters, G. W. (2020). Bayesian spatial field reconstruction with unknown distortions in sensor networks. *IEEE Transactions on Signal Processing*, 68:4336–4351.
- [36] Zhang, J., Zhao, Y., Liu, M., and Kong, L. (2019). A Tukey’s g-and-h distribution based approach with PSO for degradation reliability modeling. *Engineering Computations*, 36(5):1699–1715.
- [37] Zhang, P., Nevat, I., Peters, G. W., Septier, F., and Osborne, M. A. (2018). Spatial field reconstruction and sensor selection in heterogeneous sensor networks with stochastic energy harvesting. *IEEE Transactions on Signal Processing*, 66(9):2245–2257.
- [38] Zhang, P., Peters, G. W., Nevat, I., Xiao, G., and Tan, H.-P. (2014). Distributed event

detection in sensor networks under random spatial deployment. In *2014 IEEE Military Communications Conference*, pages 623–629.

- [39] Zhu, J., Huang, H.-C., and Wu, J. (2005). Modeling spatial-temporal binary data using Markov random fields. *Journal of Agricultural, Biological, and Environmental Statistics*, 10(2):212–225.